CHALMERS

# Evaluation of impedance tube methods - A two microphone in-situ method for road surfaces and the three microphone transfer function method for porous materials

*Masters Thesis in the Masters programme in Sound and Vibration*

MARTIN WOLKESSON

Department of Civil and Environmental Engineering
*Division of Applied Acoustics*
*Vibroacoustics Group*
CHALMERS UNIVERSITY OF TECHNOLOGY
Göteborg, Sweden 2013
MASTER'S THESIS 2012:164

MASTER'S THESIS 2012:164

# Evaluation of impedance tube methods - A two microphone in-situ method for road surfaces and the three microphone transfer function method for porous materials

Martin Wolkesson

Department of Civil and Environmental Engineering
*Division of Applied Acoustics*
*Vibroacoustics Group*
CHALMERS UNIVERSITY OF TECHNOLOGY
Göteborg, Sweden 2013

Evaluation of impedance tube methods - A two microphone in-situ method for road surfaces and the three microphone transfer function method for porous materials



Master's Thesis 2012:164

Department of Civil and Environmental Engineering
Division of Applied Acoustics
Vibroacoustics Group
Chalmers University of Technology
SE-41296 Göteborg
Sweden

Tel. +46-(0)31 772 1000

Cover:
Picture of a piece of sealant applied to a road surface. This is to ensure that the joint to the impedance tube fixture is air-tight.

Reproservice / Department of Civil and Environmental Engineering
Göteborg, Sweden 2013

Evaluation of impedance tube methods - A two microphone in-situ method for road surfaces and the three microphone transfer function method for porous materials

Master's Thesis in the Master's Programme in Sound and Vibration

MARTIN WOLKESSON
Department of Civil and Environmental Engineering
Division of Applied Acoustics
Vibroacoustics Group
Chalmers University of Technology

## Abstract

There are well-known methods to use an impedance tube with two microphones to obtain the acoustic characteristics of material samples. This setup can also be used to measure the absorption coefficient in-situ on road surfaces, as a non-destructive alternative to fit drilled out road samples into the tube. Moreover, impedance tubes can also be used to obtain the non-acoustic parameters of a porous material using multiple microphones and transfer function calculations.

In this thesis, the impedance tube measurement methods are investigated and developed to satisfy requirements in standards related to specifications of test tracks that are used for vehicle pass-by noise measurements. Measurements have been conducted to ensure the conditions for low internal loss, to investigate sealant materials and to make comparisons with related road surface measurements. An alternative transfer function method has also been investigated using three microphones. Via semiphenomenological models one would be able to obtain acoustic and non-acoustic material parameters.

The developed impedance tube measurement method can be considered as valid for in-situ measurement on road surfaces, in accordance with the current standards for noise measurements on test tracks. In comparison to previous measurement results, the developed impedance tube showed reasonable results for the in-situ method. The initial three-microphone method did however not show measurement results that were useful to obtain additional acoustic and non-acoustic material results. Additional measurements of the transfer function over the sample material showed reasonable calculation results and narrowed down possible sources of errors.

**Keywords:** Impedance tube, Kundt's tube, absorption coefficient, absorption material, open porous asphalt, ISO 10844:2011, ISO 13472-2:2011

# Acknowledgements

This thesis work was carried out between January and June of 2012 at the Division of Applied Acoustics in co-operation with the Noise and Vibration Laboratory at Volvo Group Trucks Technology, AB Volvo, in Gothenburg.

I would first of all thank my supervisor Ph.D. Anders Granlund at the Noise and Vibration Laboratory, for the opportunity to write this thesis at AB Volvo, the interpretation of the measurement standards and the practical issues related to the impedance tube equipment.

Moreover, I would like to thank my supervisor Ph.D. Patrik Andersson at Chalmers, for all the help with this thesis, especially for his knowledge to implement equations into functional features.

Special thanks to all the staff at the Noise and Vibration Laboratory, in particular Ph.D. Kaj Bodlund, Tech.Eng. Carl-Axel Carlsson, Dipl.Phys. Jona Hoffman, Ph.D. Jonas Klein, M.Sc. Erik Wennberg and M.Sc. Peter Zimmerman for always make time for my questions about acoustic theory, measurement methods and feedback of this thesis.

# Contents

# 1. Introduction

The aim of this thesis has been to investigate the possibilities to measure the sound absorption of a test track using a developed impedance tube according to recently revised standards. A secondary aim was to investigate what other possibilities there are to obtain other characteristics of absorption materials by using this impedance tube. This thesis was done in collaboration with the Noise and Vibration Laboratory at AB Volvo in Gothenburg, which has supplied equipment, test samples and know-how.

The theory behind the use of two microphones in an impedance tube will be presented in Chapter 2. The concept of impedance tube measurement can be described as measuring the reflection from an incident sound wave generated by a loudspeaker in a tube. The sample under test will alter this reflection depending on the impedance at the surface of the test sample. This setup will cause a standing wave that can be measured by the microphones in the tube to be able to calculate the normal incidence absorption coefficient, since a part of the energy in the incident sound will be absorbed and dissipated to heat within the material. This kind of measurement method is well-known and standardized methods can be applied. Furthermore, a well built impedance tube can be seen as a specifically controlled test environment at a low cost. The test material samples used are also rather cheap to produce and the amount of cut-out material is small compared to other measurement methods. Assuming some additional limitations, one can use three microphones and apply the theory described in Chapter 3, to obtain additional non-acoustic parameters derived from Biot's theory of poroelasticity. The described material parameters are presented in more detail in Chapter 4 along with separate measurement methods. The measurement results presented in this thesis were obtained using a measurement instruction [36] containing calculations according to these theory chapters.

There are regulations which specifies the noise limit for vehicles sold in the EU, measured according to methods where the vehicle is driven on a test track. This test track is constructed to ensure that the noise propagation is not dependent on the test track itself, which is achieved by an asphalt surface causing low sound absorption. The additional requirements for an impedance tube measurement method to measure in-situ on road surfaces are described in Chapter 5. Measurements were conducted, and presented in Chapter 6 and 7, to evaluate the developed impedance tube against the standardized requirements of the respective methods, followed by the summarized conclusions in Chapter 8.

# 2. Impedance tube theory - Transfer function method using two microphones

Sound radiation in an impedance tube can be described as a plane wave traveling in a duct. This is true, if one assumes that the wave length of the highest frequency is longer than the lateral tube diameter, since modes will fit the cross-section of the tube causing unwanted non-plane wave modes. For this reason, the standard ISO 10534-2:1998 [2] sets the upper frequency limit for a circular impedance tube to

$$f_u < 0.58\frac{c_0}{d} \tag{2.1}$$

where $c_0$ is the speed of sound in air and $d$ is the inner diameter of the tube.

The upper frequency is also limited by the distance between the measurement points along the tube, since one must ensure a certain phase difference of at least half a wavelength,

$$f_u < 0.45\frac{c_0}{s} \tag{2.2}$$

where $s$ is the distance in between the microphone positions, often denoted as microphone spacing.

The lowest available frequency is limited to the wavelength that are so long that the pressure at the microphones are very similar and no clear pressure difference can be measured,

$$f_l > 0.05\frac{c_0}{s} \tag{2.3}$$

With these set demands on the impedance tube, the complex sound pressure propagating in the incident and reflected direction can then be described as

$$p_I = \hat{p}_I e^{(-jk_0x+\varphi_I)}e^{j\omega t} \tag{2.4}$$

$$p_R = \hat{p}_R e^{(jk_0x+\varphi_R)}e^{j\omega t} \tag{2.5}$$

where $\hat{p}_I$ and $\hat{p}_R$ are the magnitudes of the incident and reflecting waves respectively, $\varphi_I$ and $\varphi_R$ are the phase shift of the incident and reflecting waves respectively, $k_0$ is the real wave number in air and $x$ is a position in the tube from the front surface of the sample. Hereafter are the phase and time notation included in amplitude $\hat{p}_I$ and $\hat{p}_R$.

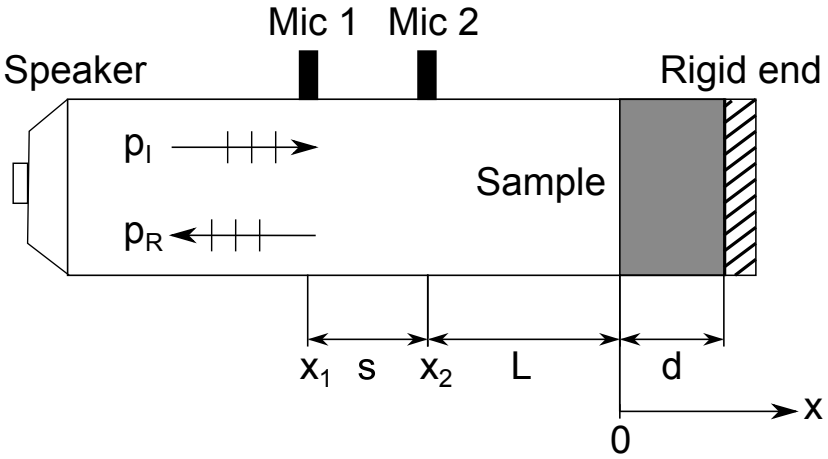


Figure 2.1.: A sketch of an impedance tube configuration for two microphones, describing the incident and reflected wave and the positions of the microphones, speaker and sample.

The complex sound pressure at the position of the microphones, see Figure 2.1, can then be calculated as

$$p_1 = p_I(x_1) + p_R(x_1) = \hat{p}_I e^{-jkx_1} + \hat{p}_R e^{jk_0 x_1} \tag{2.6}$$

$$p_2 = p_I(x_2) + p_R(x_2) = \hat{p}_I e^{jkx_2} + \hat{p}_R e^{-jk_0 x_2} \tag{2.7}$$

where $x_1$ and $x_2$ is the distance from the reference point, denoted 0 in the mentioned figure, to microphone position 1 and 2 respectively.

In order to correct for internal amplitude and phase mismatch between the microphones, one can use the microphone interchange method, also known as the microphone switching technique. This means that measurement is also conducted with the two microphones in a switched position, to obtain the transfer function between the microphones. This method opens up the opportunity to use low-cost and non-matching equipment, since the use of the transfer function will reduce minor irregularities between the microphones.

In this thesis the general form of a true transfer function is defined as in Equation 2.8. However, all the transfer functions are in practice the estimates, $\hat{H}$, of multiple single-sided auto-spectrum's, $AG$, averaged over $N$ iterations, see Equation 2.9.

$$H_{ij} = \frac{p_j}{p_i} = \frac{p_j p_i^*}{p_i p_i^*} \tag{2.8}$$

$$\hat{H}_{ij} = \frac{AG_{ij}}{AG_{ii}} = \frac{\frac{1}{N}\sum p_j p_i^*}{\frac{1}{N}\sum p_i p_i^*} \tag{2.9}$$

Moreover, the transfer function of the incident and reflecting waves between the microphone positions are defined as

$$H_I = \frac{p_I(x_2)}{p_I(x_1)} = \frac{\hat{p}_I e^{-jk_0 x_2}}{\hat{p}_I e^{-jk_0 x_1}} = e^{jk_0 s} \tag{2.10}$$

$$H_R = \frac{p_R(x_2)}{p_R(x_1)} = \frac{\hat{p}_R e^{jk_0 x_2}}{\hat{p}_R e^{jk_0 x_1}} = e^{-jk_0 s} \tag{2.11}$$

where $s = x_2 - x_1$ is the distance between the microphone positions, see Figure 2.1.

Using Equation 2.6 and 2.7, one can obtain the transfer function $H_{12}$ as

$$H_{12} = \frac{p_2}{p_1} = \frac{\hat{p}_I e^{-jk_0 x_2} + \hat{p}_R e^{jk_0 x_2}}{\hat{p}_I e^{-jk_0 x_1} + \hat{p}_R e^{jk_0 x_1}} = \frac{e^{-j(k_0 x_2 + \varphi)} + R e^{j(k_0 x_2 + \varphi)}}{e^{-j(k_0 x_1 + \varphi)} + R e^{j(k_0 x_1 + \varphi)}} \tag{2.12}$$

where $R$ denotes the reflection coefficient, defined as the ratio of the complex reflected and incident pressure. This equation can be further derived to show the reflection coefficient at microphone position 1, $x = x_1$, by including Equation 2.10 and 2.11,

$$R_{x=x_1} = \frac{H_{12} - H_I}{H_R - H_{12}} = \frac{H_{12} - e^{jk_0 s}}{e^{-jk_0 s} - H_{12}} \tag{2.13}$$

However, the reflection coefficient of interest is the one of the material, which only can be obtain at the position of the material surface $x = 0$, see Figure 2.1. An additional term must be added to Equation 2.13 to compensate for the distance from microphone 1 at $x_1$ to the surface of the sample [19],

$$\frac{R_{x=0}}{R_{x=x_1}} = \frac{e^{jk_0 x_1}}{e^{-jk_0 x_1}} \tag{2.14}$$

$$R_{x=0} = R_{x=x_1} e^{jk_0 2x_1} \tag{2.15}$$

The reflection coefficient at the sample surface, $x = 0$, can therefore be derived as

$$R = \frac{H_{12} - H_I}{H_R - H_{12}} e^{jk_0 2x_1} \tag{2.16}$$

The general definition of the sound absorption coefficient is the fraction of incident energy propagating into a sample material versus the energy propagating out. A part of the incident energy will be absorbed into the sample material, or rather converted to heat energy caused by the friction between the moving air molecules and the porous structure inside the sample material. Since the impedance tube is assumed to be an acoustically closed system, this must imply that the part of the incident propagating wave that is not reflected by the material must be absorbed, therefore

$$\alpha = 1 - |R|^2 \tag{2.17}$$

The surface impedance of the material, calculated by Equation 2.18, is often presented in real and imaginary terms respectively. The real part describes the energy losses whereas the imaginary part describes the phase changes caused by the material. [20]

$$Z_S = Z_0 \frac{1+R}{1-R} \tag{2.18}$$

where $Z_0 = \rho_0 c_0$ is the acoustical characteristic impedance of air.

# 3. Impedance tube theory - Transfer function method using three microphones

## 3.1. Acoustic characteristics

The two-microphone measurement technique can be improved to obtain further material characteristics, by an additional microphone mounted flush and air tight with the inner wall of the rigid end-piece, see Figure 3.1. Note that this method is limited to only measure homogenous and isotropic materials, i.e. the material properties must be spatial uniform independent by direction. By calculating the transfer function from both sides of the material, one is able to obtain the characteristic impedance and wave number of the material exclusively. Moreover, these measurement results can be used to obtain the equivalent bulk modulus and equivalent density of the material, based on the rigid and limp models, further described in Section 3.2.

The three-microphone measurement method was originally developed by Iwase et al. [35], however the enhanced version presented in this thesis was developed by Salissou et al. [32] that uses the similar switching microphone concept as used in the two-microphone method, see Chapter 2. This method is carried out by first measure the transfer function $H_{32}$ and then switch to $H_{31}$. The transfer function $H_{12}$, that corresponds to the one presented in the two-microphone method, can be obtained by

$$H_{12} = \frac{H_{32}}{H_{31}} \tag{3.1}$$

which allows one to avoid moving the microphone mounted in the rigid end-piece.

The transfer function, $H_{30}$, from the surface of the material, $x = 0$, to the rigid end-piece, $x = x_3$, cannot be directly obtained using the evaluated measurement set-up, however calculated by

$$H_{30} = \frac{p_0}{p_3} = \frac{p_0}{p_2}\frac{p_2}{p_3} = \frac{p_0}{p_2}H_{32} =$$

$$= \frac{\hat{p}_I + \hat{p}_R}{\hat{p}_I e^{-jk_0x_2} + \hat{p}_R e^{jk_0x_2}}H_{32} = \frac{1+R}{e^{-jk_0x_2} + Re^{jk_0x_2}}H_{32} \tag{3.2}$$

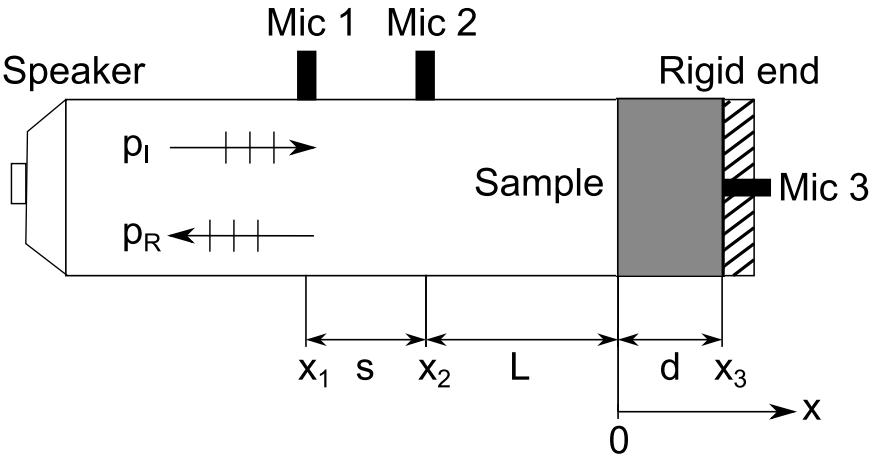


Figure 3.1.: A sketch of an impedance tube configuration for three microphones, describing the incident and reflected wave and the positions of the microphones, speaker and sample.

where $R$ is the reflection coefficient at position $x = 0$, as calculated in Equation 2.16, and $H_{32}$ is the transfer function between microphone 2 and 3, including a compensation for the distances between the sample surface and microphone 2, $L$, and the depth or thickness of the material sample, $d$,

$$H_{32} = \frac{H_{32,x_2} - e^{jk_0(L+d)}}{e^{-jk_0(L+x_3)} - H_{32,x_2}} \tag{3.3}$$

where the subscript $x_2$ denotes reference position of the transfer function.

The reflection coefficient, absorption coefficient and surface impedance can be calculated by Equation 2.16 to 2.18, using the transfer function $H_{12}$, see Equation 3.1. This latter equation requires the transfer function $H_{31}$ calculated to including a compensation for the distance between the microphones, $s$,

$$H_{31} = \frac{H_{31,x_1} - e^{jk_0(s+L+d)}}{e^{-jk_0(s+L+x_3)} - H_{31,x_1}} \tag{3.4}$$

where the subscript $x_1$ denotes reference position of the transfer function.

Allard et al. [12] described a transfer matrix method relating the sound pressures and air particle velocities on both sides of a material sample

$$\begin{bmatrix} p_0 \\ v_0 \end{bmatrix} = \begin{bmatrix} T_{11} & T_{12} \\ T_{21} & T_{22} \end{bmatrix} \begin{bmatrix} p_{x_3} \\ v_{x_3} \end{bmatrix} \tag{3.5}$$

where the transfer matrix elements $T$ are the transmission coefficients. Song et al. [34] were also able to show two additional equations describing that if the sample is sym-

metrical and reciprocal in $x$ direction, described in Equations 3.6 and 3.7 respectively, the first transfer matrix element can be reduced to equal the previously shown transfer function over the sample, $H_{30}$, since the air particle velocity at the rigid end-piece can be defined to $v_{x_3} = 0$, see Equation 3.8,

$$T_{11} = T_{22} \tag{3.6}$$

$$T_{11}T_{22} - T_{21}T_{12} = 1 \tag{3.7}$$

$$T_{11} = \frac{p_{x_3}v_{x_3} + p_0v_0}{p_0v_{x_3} + p_{x_3}v_0} = \frac{p_0v_0}{p_{x_3}v_0} = H_{30} \tag{3.8}$$

Allard et al. [12] show that if one is considering a finite depth layer and homogeneous isotropic material one can calculate the complex wave number and characteristic impedance using models for limp or rigid materials,

$$\begin{bmatrix} T_{11} & T_{12} \\ T_{21} & T_{22} \end{bmatrix} = \begin{bmatrix} \cos(k_m d) & j\sin(k_m d)Z_0 \\ j\sin(k_m d)/Z_0 & \cos(k_m d) \end{bmatrix} \tag{3.9}$$

where $k_m$ is the complex wave number of the air inside the material. The latter can be derived, as described by Salissou et al. [32], considering Equation 3.8 and the substitution made in Equation 3.2,

$$k_m = \frac{1}{d}\cos^{-1}(H_{30}) = \frac{1}{d}\cos^{-1}\left(\frac{1+R}{e^{-jk_0x_2} + Re^{jk_0x_2}}H_{32}\right) \tag{3.10}$$

where $H_{30}$ is the transfer function previously derived in Equation 3.2.

Using the mentioned models, one is also able to obtain the surface impedance, $Z_s$, and the characteristic impedance of the material, $Z_c$.

$$Z_s = Z_c\coth(jk_m d) \tag{3.11}$$

$$Z_c = \frac{Z_s}{\coth(jk_m d)} = Z_s\tanh(jk_m d) = -jZ_s\tan(k_m d) \tag{3.12}$$

Doutres et al. [21] have also shown an expression to calculate the transmission coefficient from the mentioned parameters

$$\tau_\infty = 2j\frac{Z_c}{Z_0 - 2jZ_c\cot(k_m d) + Z_c^2/Z_0}\frac{1}{\sin(k_m d)}e^{jk_0 d} \tag{3.13}$$

One can also derive a relation between the characteristic impedance and complex wave number to the effective density, $\rho_{eff}$ , effective bulk modulus, $K_{eff}$,

$$Z_c = \sqrt{K_{eff}\rho_{eff}} \tag{3.14}$$

$$k_m = \omega\sqrt{\frac{\rho_{eff}}{K_{eff}}} \tag{3.15}$$

describing the respective material property as experienced by the propagating wave, rather than by direct measurement of the normal and well-known density and bulk modulus definitions [12]. Both quantities are useful as inputs in various porous absorption prediction models and are often given in material data specifications. Moreover, Doutres et al.[21] described a relation to indirect calculate the effective density and effective bulk modulus,

$$\rho_{eff} = \frac{\phi Z_C k_m}{\omega} \tag{3.16}$$

$$K_{eff} = \frac{\phi Z_C \omega}{k_m} \tag{3.17}$$

where $\phi$ is the porosity and $\omega = 2\pi f$ is the angular frequency.

## 3.2. Non-acoustic characteristics

Allard et al.[12] and Atalla et al. [14] describe that the classical Biot theory [15][16] can be used to model homogenous and isotropic poroelastic materials in FEM calculations using Biot's poroelasticity equations. This theory is a complete description of the motion and strain tensors of the fluid and the porous skeleton of the porous material. However, these type of calculations are complex and not very computational efficient. To model a three dimensional structure, one would need four or six DOF per node, depending on the model. The scope of this thesis is not to benchmark the validity of various FEM calculations, rather to show how the Biot theory can be used to obtain non-acoustic parameters that can be indirectly measured using an impedance tube. This section will provide as a background to the theory behind the limp and rigid limited models and the associated assumptions and limitations. These include, besides material parameters, the effective density and effective bulk modulus that was previously mentioned in Equation 3.14 to 3.17, and can be used to model absorption characteristics of a material in the design-stage.

### 3.2.1. The mixed displacement pressure formulation based on the Biot theory

Biot's theory is describing the so-called elastic frame model, where three waves are considered to propagate inside the porous material: the elastic compression wave, the acoustic compression wave and the elastic shear wave. Further assumptions are that the porosity is uniform throughout the material, which is the case for most porous materials on a macroscopic level, i.e. the skeleton pore sizes are much smaller than the longest wavelength of interest.

Atalla et al. [14] describe the displacement formulation of the coupled Biot poroelasticity equations as derived from the classical equation of motion in elastic solids,

$$\begin{cases} \operatorname{div} \sigma^s = \rho_{11}\ddot{\mathbf{u}}^s + \rho_{12}\ddot{\mathbf{u}}^f + \tilde{b}\left(\dot{\mathbf{u}}^s - \dot{\mathbf{u}}^f\right) \\ \operatorname{div} \sigma^f = \rho_{22}\ddot{\mathbf{u}}^f + \rho_{12}\ddot{\mathbf{u}}^s - \tilde{b}\left(\dot{\mathbf{u}}^s - \dot{\mathbf{u}}^f\right) \end{cases} \tag{3.18}$$

where $\mathbf{u}^s$ and $\mathbf{u}^f$ are the microscopic displacement vectors of the solid and fluid phase respectively, $\sigma^s$ denotes the partial stress for the aggregate particles of the skeleton material and $\sigma^f = -\phi p$ the partial stress related to the average pressure prevailing in the fluid, e.g. air inside the material, $\phi$ is the porosity of the poroelastic material. The viscous damping coefficient, $\tilde{b}$, can be related to the flow resistivity of the material. The tilde sign, $\tilde{}$, denotes that the coefficients account for damping and frequency dependence. The densities $\rho_{11}$ and $\rho_{22}$ are mass coefficients based on the fact that the flow through the pores is not uniform, related to the mass density of the solid material, $\rho_s$, and the fluid, $\rho_0$. The density $\rho_{12}$ can be described as an interaction coefficient for the inertia forces of the solid and fluid phases,

$$\rho_{11} = (1-\phi)\rho_s - \rho_{12} \tag{3.19}$$

$$\rho_{22} = \phi\rho_0 - \rho_{12} \tag{3.20}$$

From the mentioned Biot's displacement formulation, Allard et al. [12] have derived an exact mixed displacement-pressure formulation,

$$\begin{cases} \omega^2\tilde{\rho}_{11}\mathbf{u}^s + \omega^2\tilde{\rho}_{12}\mathbf{u}^f + \operatorname{div}\sigma^s = 0 \\ \omega^2\tilde{\rho}_{22}\mathbf{u}^f + \omega^2\tilde{\rho}_{12}\mathbf{u}^s - \phi\,\nabla p = 0 \end{cases} \tag{3.21}$$

Assuming a harmonic time dependence, $e^{j\omega t}$, the complex effective densities can be described as

$$\tilde{\rho}_{11} = \rho_{11} + \frac{\tilde{b}}{j\omega} \tag{3.22}$$

$$\tilde{\rho}_{22} = \rho_{22} + \frac{\tilde{b}}{j\omega} \tag{3.23}$$

$$\tilde{\rho}_{12} = \rho_{12} - \frac{\tilde{b}}{j\omega} \tag{3.24}$$

The second equation in Equation 3.21 can be expressed as,

$$\mathbf{u}^f = \frac{\phi}{\omega^2 \tilde{\rho}_{22}} \nabla p - \frac{\tilde{\rho}_{12}}{\tilde{\rho}_{22}} \mathbf{u}^s = 0 \tag{3.25}$$

and by replacing the first equation in Equation 3.21,

$$\omega^2 \tilde{\rho} \mathbf{u}^s + \phi \frac{\tilde{\rho}_{12}}{\tilde{\rho}_{22}} \nabla p + \operatorname{div} \sigma^s = 0 \tag{3.26}$$

where the effective density, $\tilde{\rho}$, is expressed as

$$\tilde{\rho} = \tilde{\rho}_{11} - \frac{(\tilde{\rho}_{12})^2}{\tilde{\rho}_{22}} \tag{3.27}$$

### 3.2.2. Solid phase equation in terms of solid phase displacement and the pressure

The Equation 3.26 however is not only dependent on the solid phase displacement $\mathbf{u}^s$ and the pressure $p$ as wanted but also dependent on the fluid phase displacement, $\sigma^s = \sigma^s(\mathbf{u}^s, \mathbf{u}^f)$. In the Biot theory there is a stress-strain relation

$$\begin{cases} \sigma^s(\mathbf{u}^s, \mathbf{u}^f) = \tilde{A} \operatorname{div} \mathbf{u}^s \mathbf{I} + 2N\varepsilon^s + \tilde{Q} \operatorname{div} \mathbf{u}^f \mathbf{I} \\ -\phi p 1 = \tilde{R} \operatorname{div} \mathbf{u}^f \mathbf{I} + \tilde{Q} \operatorname{div} \mathbf{u}^s \mathbf{I} \end{cases} \tag{3.28}$$

where $\mathbf{I}$ is the identity tensor, $\tilde{A}$ and $N$ are the Lam coefficients for elastic solids, $\tilde{Q}$ is the potential coupling coefficient and $\tilde{R} = \phi \tilde{K}_f$. One can further express the elastic coefficients $\tilde{A}$, $\tilde{Q}$ and $\tilde{R}$ with dependencies of the bulk modulus of the skeleton in vacuum, $K_b$, the bulk modulus of the elastic solid, $K_s$, and the bulk modulus of the air in the pores, $\tilde{K}_f$,

$$\tilde{A} = \frac{(1-\phi)(1-\phi-K_b/K_s)K_s + \phi\left(K_s/\tilde{K}_f\right)K_b}{1-\phi-K_b/K_s+\phi K_s/\tilde{K}_f} - \frac{2}{3}N \tag{3.29}$$

$$\tilde{Q} = \frac{(1-\phi-K_b/K_s)\phi K_s}{1-\phi-K_b/K_s+\phi K_s/\tilde{K}_f} \tag{3.30}$$

$$\tilde{R} = \frac{\phi^2 K_s}{1 - \phi - K_b/K_s + \phi K_s/\tilde{K}_f} \tag{3.31}$$

where $N$ in this case denotes the shear modulus of the skeleton in vacuum including the structural damping.

Now, by combing the coupled equations in Equation 3.28 one can define the variable $\hat{\sigma}^s$, that only depends on the solid phase displacement vector

$$\sigma^s(\mathbf{u}^s, \mathbf{u}^f) = \left(\tilde{A} - \frac{\tilde{Q}^2}{\tilde{R}}\right) \operatorname{div} \mathbf{u}^s \mathbf{I} + 2N\varepsilon^s - \phi\frac{\tilde{Q}}{\tilde{R}} p\mathbf{I} = \hat{\sigma}^s(\mathbf{u}^s) - \phi\frac{\tilde{Q}}{\tilde{R}} p\mathbf{I} \tag{3.32}$$

$$\hat{\sigma}^s(\mathbf{u}^s) = \left(\tilde{A} - \frac{\tilde{Q}^2}{\tilde{R}}\right) \operatorname{div} \mathbf{u}^s \mathbf{I} + 2N\varepsilon^s \tag{3.33}$$

By substituting Equation 3.33 into Equation 3.26 the mentioned fluid phase displacement dependency is eliminated. The solid phase equation in terms of the solid phase displacement $\mathbf{u}^s$and the pressure $p$, can now be expressed as

$$\operatorname{div} \hat{\sigma}^s(\mathbf{u}^s) + \omega^2 \tilde{\rho} \mathbf{u}^s + \tilde{\gamma} \nabla p = 0 \tag{3.34}$$

where $\tilde{\gamma}$ is the volume coupling coefficient,

$$\tilde{\gamma} = \phi\left(\frac{\rho_{12}}{\rho_{22}} - \frac{\tilde{Q}}{\tilde{R}}\right) \tag{3.35}$$

### 3.2.3. Fluid phase equation in terms of solid phase displacement and the pressure

One can take the divergence of Equation 3.25

$$\operatorname{div} \mathbf{u}^f = \frac{\phi}{\omega^2 \tilde{\rho}_{22}} \Delta p - \frac{\tilde{\rho}_{12}}{\tilde{\rho}_{22}} \operatorname{div} \mathbf{u}^s = 0 \tag{3.36}$$

where $\Delta$ is the Laplace operator, with the second equation in Equation 3.21 one will obtain the fluid phase equation in terms of solid phase displacement and the pressure, expressed as

$$\Delta p + \frac{\tilde{\rho}_{22}}{\tilde{R}} \omega^2 \tilde{\rho} + \frac{\tilde{\rho}_{22}}{\phi^2} \tilde{\gamma} \omega^2 \operatorname{div} \mathbf{u}^s = 0 \tag{3.37}$$

### 3.2.4. Poroelasticity equation in terms of solid phase displacement and the pressure

Now, by combining the solid phase equation and the fluid phase equation, see Equation 3.34 and 3.37 respectively, one is able to express the Biot poroelasticity equation, see Equation 3.18, in terms of solid phase displacement and pressure

$$\begin{cases} \operatorname{div} \hat{\sigma}^s(\mathbf{u}^s) + \omega^2 \tilde{\rho} \mathbf{u}^s + \tilde{\gamma} \nabla p = 0 \\ \Delta p + \frac{\tilde{\rho}_{22}}{\tilde{R}} \omega^2 \tilde{\rho} + \frac{\tilde{\rho}_{22}}{\phi^2} \tilde{\gamma} \omega^2 \operatorname{div} \mathbf{u}^s = 0 \end{cases} \tag{3.38}$$

Panneton [29] present an alternative set of coupled equations, see Equation 3.39, that can be related via equivalent fluid models or other semiphenomenological models to non-acoustic parameters. Here, the first two terms in both equations are respectively representing the dynamic behavior of the solid material in vacuum and the dynamic behavior of the fluid when the frame is rigid. The third term in both equations couples the dynamics of the solid and fluid phases.

$$\begin{cases} \operatorname{div} \hat{\sigma}^s(\mathbf{u}^s) + \omega^2 \tilde{\rho}_s \mathbf{u}^s + \tilde{\gamma} \nabla p = 0 \\ \frac{\phi}{\omega^2 \rho_{eff}} \Delta p + \frac{\phi}{K_{eff}} p - \gamma \operatorname{div} \mathbf{u}^s = 0 \end{cases} \tag{3.39}$$

where $\gamma$ is the volume coupling coefficient and $\rho_s$ the effective solid phase density, both complex and will vary with frequency, expressed as

$$\gamma = \frac{\phi \rho_0}{\rho_{eff}} + \frac{K_b}{K_s} - 1 \tag{3.40}$$

$$\rho_s = \rho_1 + \phi \rho_0 \left( 1 - \frac{\rho_0}{\rho_f} \right) \tag{3.41}$$

where $K_s$ is the bulk modulus of the elastic frame material, $K_b$ is the bulk modulus of the frame material in vacuum and $\rho_1$ is the bulk density of the material in vacuum.

### 3.2.5. Rigid frame limitation model

Panneton [29] describes that the rigid frame model is assuming a motionless rigid frame material, i.e. the frame displacement is $u = 0$. This imply that the first coupled equation in Equation 3.39 will be neglected and the second equation is reduced to form a simplified Helmholtz equation,

$$\Delta p + \frac{\rho_{eq}}{K_{eq}} \omega^2 p = 0 \tag{3.42}$$

where $\rho_{eq} = \frac{\rho_{eff}}{\phi}$ is the effective density and $K_{eq} = \frac{K_{eff}}{\phi}$ is the effective bulk modulus.

This simple model is used for rigid and heavy porous materials, where one assume no elastic coupling between the fluid and solid frame and only the acoustic compression wave propagation is concerned. The characteristics of the material is, in this model, mainly dependent on the geometry and the orientation of these pores [24]. For fibrous materials the frames are defined as long, thin and cylindrical strings of rigid material, where as for granular material frame material is assumed to be spherical rocks, aggregates or sediments that are packed to contain inter-connected air pockets.

### 3.2.6. Limp frame limitation model

Panneton [29] also describe that the limp model assumes that the porous material is flexible and do not make any resistance to external excitations, so the stiffness of the frame can be neglected, i.e. the bulk modulus of the frame in vacuum is approximated to zero, $K_b \approx 0$ . Also, the stress tensor of solid phase is neglected , $\hat{\sigma}^s \approx 0$. In the poroelasticity equation, see Equation 3.39, the first equation will be reduced to $\omega^2 \rho_s \, div\, \mathbf{u}^s + \gamma \, \Delta p = 0$. By substituting this equation to the second equation in Equation 3.39, one will obtain the so-called limp frame equivalent fluid equation,

$$\Delta p + \frac{\rho_{eq,limp}}{K_{eq}} \omega^2 p = 0 \tag{3.43}$$

where $K_{eq}$ is the equivalent bulk modulus as used in the rigid frame model and $\rho_{eq,limp}$ is the equivalent limp density,

$$\rho_{eq,limp} = \frac{\rho_s \rho_{eq}}{\rho_s + \rho_{eq} \gamma^2} \tag{3.44}$$

If one assumes that the bulk modulus of the elastic material is much larger than the bulk modulus of the frame, $K_b \ll K_s$, which is the case for most porous materials, the equivalent limp density can be approximated by

$$\rho_{eq,limp} \approx \frac{\rho_t \rho_{eq} - \rho_0^2}{\rho_t + \rho_{eq} - 2\rho_0} \tag{3.45}$$

where $\rho_t = \rho_1 + \phi \rho_0$ is the total density of the equivalent fluid limp material.

### 3.2.7. Comparison of the rigid and limp frame limitation models

The mentioned effective quantities can be used to calculate the complex equivalent characteristic impedance and complex equivalent wave number, see Equation 3.14 and 3.15 respectively. By accepting the assumptions for the respective model, one is able to use these effective quantities in the transfer matrix, see Equation 3.9, to further calculate various acoustic parameters, such as the complex wave number and surface impedance.

The rigid frame model is suggested [12] [29] to be used when the material frame is heavy and the porous material is freely suspended, i.e. no rigid body motion. The limp frame model are rather used when the material is constrained or mounted to a structure. In the case of an impedance tube measurement, the limp model is often preferred since the measurement requires that the sample is constrained, however still free to move inside the tube, i.e. sliding boundary conditions, and that the sample is set flush with the rigid end-piece. The limp model have also shown a better correlation with measurements in the lower frequency range.

Another suggested rule of thumb given in [12] is to use the limp frame model when the bulk modulus ratio between the medias are

$$\frac{K_c}{K_f} < 0.2 \tag{3.46}$$

where $K_c$ and $K_f$ are the bulk modulus of the fluid in the pores and the bulk modulus of the frame in vacuum, respectively. Since the fluid in our case is air, with an isothermal value of approximately 100 kPa, one should consequently use the limp frame model when $K_f$ is lower than 20 kPa.

### 3.2.8. Semiphenomenological models to relate to non-acoustic parameters

The limp and rigid frame modeled effective densities can be approximated by simulation in various semiphenomenological models. The model presented in Johnson et al. [23] has been shown to be accurate in comparison with measurements [29],

$$\rho_{eq,Johnson} = \frac{\rho_0 \alpha_\infty}{\phi}\left(1 - j\frac{\sigma\phi}{\omega\rho_0\alpha_\infty}\sqrt{1 + j\frac{4\alpha_\infty^2\eta\rho_0}{\sigma^2\phi^2\Lambda^2}\omega}\right) \tag{3.47}$$

where $\rho_0$ is the density of air, $\sigma$ is the static flow resistivity of the material, $\alpha_\infty$ is the tortuosity of the material, $\Lambda$, viscous characteristic length and $\eta \approx 1.81 \cdot 10^{-5}$ is the air viscosity at the temperature of $20^\circ C$ .

Since the effective density already can be obtained by impedance tube measurements, one are able to use this model to derive further parameters by using analytical inversion methods. Key to these calculations are to separate the complex parts of the mentioned effective density, see Equation 3.47. The static flow resistivity, $\sigma$, denotes the pressure difference the air flow encounters when passing through the material, i.e. at 0 Hz. One is able to obtain an approximation for this quantity by using Equation 3.48, with a reasonable accuracy of approximately 20 % [20], if data is gathered for a sufficiently low frequency,

$$\sigma = -\frac{1}{\phi}\lim_{\omega\to 0}\left(\mathrm{Im}(\omega\rho_{eq})\right) \tag{3.48}$$

Moreover is one able to derive the tortuosity, $\alpha_\infty$, viscous characteristic length, $\Lambda$, and thermal characteristic length, $\Lambda'$, see Equation 3.49 to 3.51. The latter two parameters are depending on the micro-geometries of the frame material and describing the viscous and thermal dissipation phenomena in porous materials, in detail described by Panneton and Olny [20] [30]. To be used in macroscopic models, they are often obtained by calculations since the hard nature to measure them. In the mentioned models, they are presented as

$$\alpha_\infty = \frac{1}{\rho_0}\left(\mathrm{Re}(\rho_{eq}) - \sqrt{\mathrm{Im}(\rho_{eq})^2 - \left(\frac{\sigma\phi}{\omega}\right)^2}\right) \tag{3.49}$$

$$\Lambda = \alpha_\infty \sqrt{\frac{2\rho_0\eta}{\omega \mathrm{Im}(\rho_{eq})(\rho_0\alpha_\infty - \mathrm{Re}(\rho_{eq}))}} \tag{3.50}$$

$$\Lambda' = \delta_t\sqrt{2}\left(-\mathrm{Im}\left(\left(\frac{\phi - \frac{K}{K_a}}{\phi - \gamma\frac{K}{K_a}}\right)^2\right)\right)^{-1/2} \tag{3.51}$$

where $K_a$ is the adiabatic bulk modulus, $\gamma = 1.01$ is the ratio of specific heat in air, $\delta_t = \sqrt{\frac{2\eta}{\rho_0\omega P_r}}$ is the Prandtl number where $P_r = 0.77$ at the temperature of 20 $^\circ C$.[28]

### 3.2.9. The Delany-Bazley empirical model

Delany and Bazley have derived an empirical model that estimates the complex wave number and characteristic impedance of a material [31]:

$$k_{m,DB} = \frac{\omega}{c_0}\left(1 + 0.0978\left(\frac{\rho_0 f}{\sigma}\right)^{-0.7} - j0.189\left(\frac{\rho_0 f}{\sigma}\right)^{-0.595}\right) \tag{3.52}$$

$$Z_{c,DB} = \rho c_0\left(1 + 0.0571\left(\frac{\rho_0 f}{\sigma}\right)^{-0.754} - j0.087\left(\frac{\rho_0 f}{\sigma}\right)^{-0.732}\right) \tag{3.53}$$

This model is well-known and often used for a to preliminary investigation of the acoustic characteristics of fibrous absorption materials. The model is based on the function of density of the air multiplied with the quotient of the frequency and flow resistivity. This latter quotient should be inside the limits of $10 \leq \frac{f}{\sigma} \leq 1000$, for this model, to be inside the range of validity [31].

# 4. Absorption material parameters

## 4.1. Production of material samples

The theory presented in Chapter 2 or 3 only considers normal incidence measurement cases. The shape of the front surface of the sample should therefore not be of any wedged or extreme shape, since one must be able to define a mean sample thickness. The back surface must however be flat, since any cavities will create an unwanted Helmholtz resonator. The cut-out of the samples must be done with high precision, since the samples must be cylindrical and straight cut with preferably flat and parallel surfaces, see reference [36] for a more extensive description of the production of material samples.

## 4.2. Static flow resistivity

To be able to obtain sound absorption inside a material, the inner structure of the material must reduce the wave propagation intensity. This transformation of sound energy to heat energy is analogous to how well the air flow is able to pass through the material. The static flow resistivity is a parameter that can be described as the pressure difference the air flow encounters when passing through the material. The internal microscopical material structure is key to what extent a material is able to absorb sound. The flow resistivity is commonly measured by the direct or alternating air flow methods described in ISO 29053:1993 [9], see Figure 4.1.

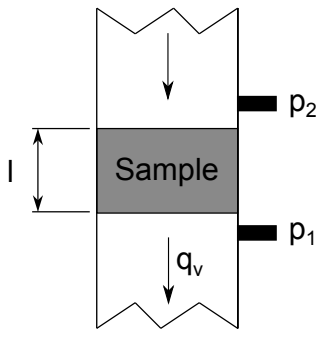


Figure 4.1.: Sketch of the direct air flow method to measure the flow resistivity.

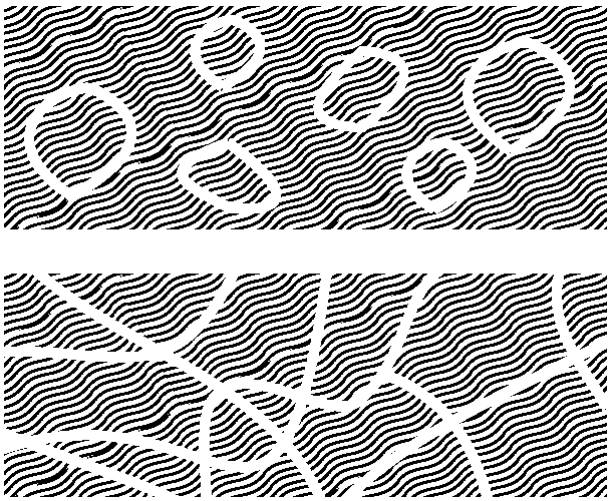

Figure 4.2.: Sketch of the difference between open and closed pores in the material structures.

The direct method is based on the pressure drop difference between the sample material and the reference material. This pressure difference over the material $\Delta p_2 = p_b - p_a$ is then used to be able to calculate the static flow resistivity to

$$\sigma = R_1 \frac{\Delta p_2}{\Delta p_1} \frac{S}{l} \tag{4.1}$$

where $R_1$ is the measured flow resistance of a reference material, $\Delta p_1$ is the pressure drop over the reference material, $S$ is the cross-section area and $l$ is the length or thickness of the material. The mentioned standard defines $q_v = 0.5 \cdot 10^{-3}$ m/s as the constant air flow rate through the material sample under test.

## 4.3. Porosity

Porosity is defined as the fraction of air volume occupied inside a total material volume, often also denoted as open porosity. This parameter might seem straightforward, however keep in mind that in some materials, like cell foams, many pores are closed and no air-flow is passing through the material. A material is considered sound absorptive if the pores are inter-connected and therefore allow air flow. In this sense, one can also understand that fibrous materials often have an open porosity close to unity and open porous asphalt surface layers of 0.20, see Figure 4.2. [20]

The open porosity can be measured by using a piston that alters the pressure $V_{ext}$ in a container and the pressure difference $\Delta p$ is measured at the connection to a volume

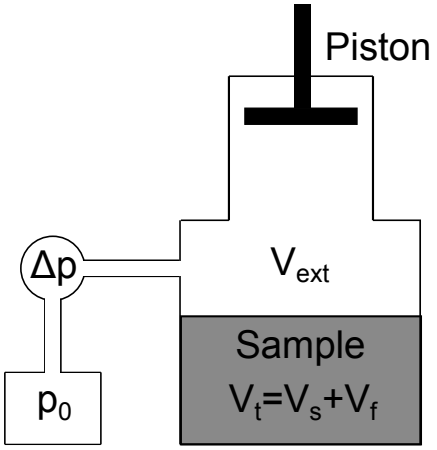


Figure 4.3.: Sketch of the work principle of a porosimeter.

with initially static pressure $p_0$. By applying the Boyle-Mariotte law for perfect gases, $pV = cte$, one is able to calculate the volume of the air in the material to

$$V_f = -\left(\frac{p_0 + \Delta p}{\Delta p}\Delta V + V_{ext}\right) \tag{4.2}$$

and to calculate the open porosity by

$$\phi = \frac{V_f}{V_t} \tag{4.3}$$

where $V_t$ is the volume of the sample, see sketch in Figure 4.3. Another standardized measurement procedure for can also be found in ASTM D6226 and ISO 4590:2000, where the latter is exclusively for measuring on cellular materials [31].

## 4.4. Tortuosity

Tortuosity describes the relation between the length of the actual path and the direct path of the air flow passing through the material. The word itself can be explained as a tortuous and twisted shape, and some are denoting this parameter as form factor. In case of measuring this parameter in an impedance tube for an anisotropic material, one need to notice that the outcome is most dependent on the orientation of the pores inside the material relative to the normal incident sound waves. This parameter is key for a material with high sound absorption, since different inner structural material geometries with different pore shapes can absorb sound more or less efficient. If the flow through the material is complex with a low flow resistance, i.e. the pores are not considered as straight cylindrical tubes, the material will absorb more efficient [20].

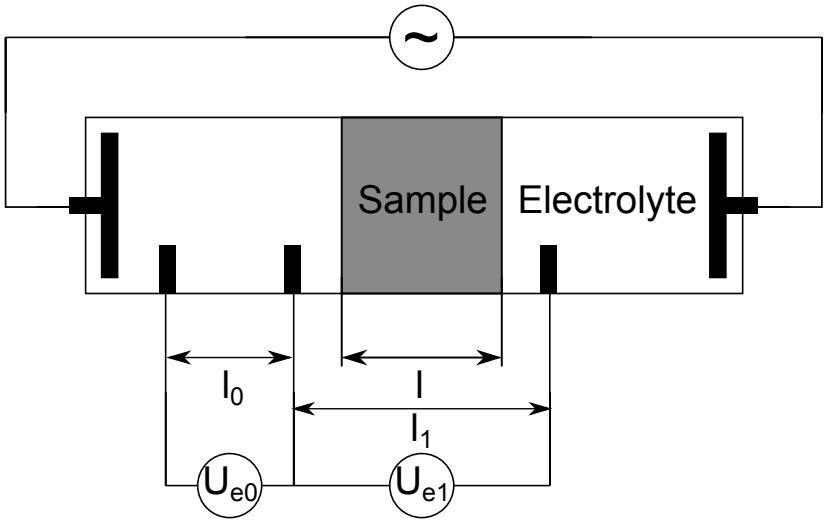


Figure 4.4.: Sketch of the principle of an tortuosity meter

This parameter can be measured by saturating the material with a conductive non-viscous fluid and measuring the resistivity between two electrode plates on each side of the material [31], see Figure 4.4. The resistivity can, as an analogy to electrical circuits, be seen as multiple parallel and serial connected resistors made up of the interconnected saturated pores. The tortuosity can then be calculated as

$$\alpha_\infty = \phi \frac{R_e}{R_{e0}} \tag{4.4}$$

where $R_e$ and $R_{e0}$ is the resistivity measured with and without the sample respectively. This resistivity relation can be calculated to

$$\frac{R_e}{R_{e0}} = 1 - \frac{l_I}{l} + \frac{U_{e1} l_0}{U_{e0} l} \tag{4.5}$$

where $U_{e1}$ and $U_{e0}$ are the voltages in the respective electrodes and $l$ and $l_0$ the lengths which can be read out by referring to Figure 4.4.

# 5. Measurement related to ISO standard test tracks

## 5.1. Introduction

The ECE Regulation 51 [11] specifies the noise limit for vehicles sold in the EU. It specifies that the method in ISO 362-1 [10] should be performed to measure the noise emission from an accelerating driving-by vehicle, as typically under urban traffic conditions. To make the measurements comparable between test sites it is required to construct the test surface area so that the noise propagation is not dependent on the road surface, see a sketch in Figure 5.1. This can be achieved by using surface properties causing low sound absorption, to reflect the noise from various sources of the vehicle. This means that the asphalt surface layer should not be of an open porous asphalt, OPA, rather a dense asphalt concrete, DAC, in which the aggregate is of an interlocking structure, not to create inter-connecting pores in the surface layer causing unwanted sound absorption.

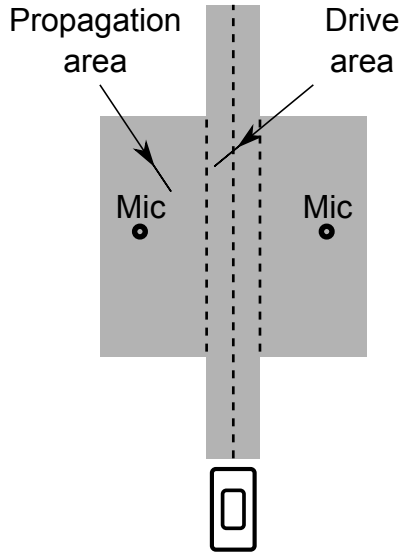


Figure 5.1.: Sketch of the test track as specified in ISO 10844.

The design specifications for this type of test track are given in ISO 10844 [3] [4] demanding the average absorption coefficient not to exceed a given value, see Section 5.2. According to these mentioned standards, the absorption coefficient should be measured, according to ISO 10534-1:1996 [1] and ISO 13472-2:2011 [6], on drilled out samples in an impedance tube and to use the impedance tube in-situ to measure on top of the surface layer respectively, see Section 5.3. ISO 10844 [3] [4] also mentions alternative methods to relate the noise emission to the surface layer. One is to measure the residual void content, which is similar to porosity; the ratio of air to asphalt, see Section 5.4. Another method is to either perform the sand-patch method or estimate the texture depth by scanning, see Section 5.5 and 5.6 respectively.

## 5.2. Comparison of ISO 10844:1994 and ISO 10844:2011

The standard ISO10844:1994 [3] specifies a method with drilled out samples to measure and calculate the residual void content and the mean sound absorption coefficient. The standard demands that *either* one of these fulfills the requirements of 0.08 and 0.10 respectively, since it was thought that the residual void content parameter was familiar and preferred by road constructors, see further description in Section 5.4. The sound absorption coefficient should, according this standard, be measured by fitting the drilled out sample in an impedance tube and using the standing wave ratio method as specified in ISO 10534-1:1996 [1]. The result is calculated by averaging the highest third-octave band absorption coefficient in the two ranges 400 Hz to 800 Hz and 800 Hz to 1600 Hz for each of the drilled out samples. These two ranges are then averaged for all the samples to represent the measured absorption coefficient. In addition to these requirements, the ISO 10844:1994 standard requires a measurement of the mean texture depth, $MTD$, to be equal to or greater than 0.4 mm, using the volumetric patch method.

The standard have been revised to ISO 10844:2011 [4], including more restrictive construction and measurement specifications to be able to reduce the variation between test sites. The sound absorption coefficient shall be measured in-situ on the asphalt surface layer according to ISO 13472-2 [6]. The requirements in ISO 10844:2011 are that the mean sound absorption coefficients should be equal to or less than 0.08 and 0.10 in the drive lane and propagation area respectively. These demands should be fulfilled by each third-octave band in the range from 315 Hz to 1600 Hz. The mean profile depth, $MPD$, should be measured to be 0.5 mm $\pm$ 0.2 mm for eight sections in the driving lane, with equipment specified in ISO 13473-1, see further in section 5.6. Furthermore, any road surface irregularities should be measured with a 3 m straightedge to ensure no irregularities over 2 mm, according to EN 13036-7:2003 [5]. The expected pass-by noise level difference, $END_T$, can be used to estimate the noise level by comparing the measured texture profile data with a given reference.

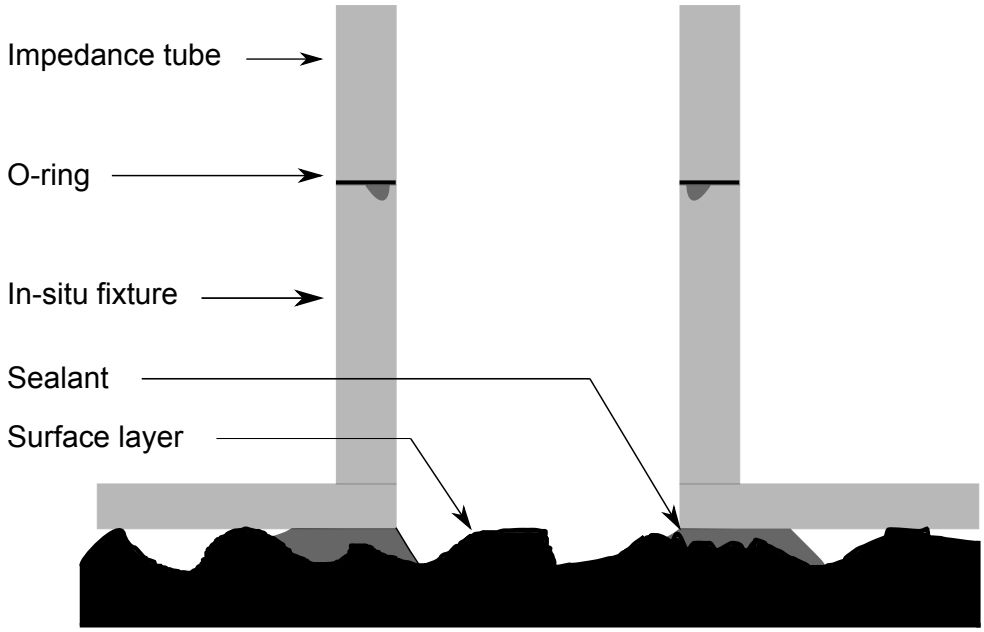


Figure 5.2.: Sketch of a typical in-situ test fixture.

## 5.3. Impedance tube measurement method in-situ according to ISO 13472-2:2011

The measurement method specified in ISO 13472-2:2011 [6] is closely related to ISO 10534-2:1998, with a similar microphone switching technique and signal processing. ISO 13472-2:2011 is specifically used when measurements are conducted in-situ on a road surface, without damaging the road surface when drilling out core samples. The ISO 13472-2:2011 requires specific dimensions of the tube, microphone positions and in-situ test fixture end-piece, as specified further down. The purpose of this standard is to measure on top of smooth reflective surface layers, such as specified by ISO 10844:2011, where the absorption do not exceed 0.15. Moreover, in this standard there is an added demand of a reference base accounting for loose sealing and other irregularities of the inner-wall. This empty tube reference is accomplished by a measurement on a totally reflective sample, e.g. a thick steel plate. The absorption coefficient for this test sample must be measured to be less than 0.03 in each third-octave band. This reference base is considered as parasitic absorption of the tube that should be subtracted from the measurement results. One must also ensure that the background noise level is not interfering with an ongoing measurement, hence, one should perform a SNR level measurement without a switched on noise source, to meet the requirement of 10 dB in each third-octave octave band.

ISO 13472-2:2011 requires that the measurement result is presented as third-octave bands with the center frequencies from 250 to 1600 Hz. The dimensions of the impedance tube defines the available measurement frequency range calculated according to ISO 10534-2:1998, see Section 2. However ISO 13472-2:2011 requires an inner tube diameter of 100 mm, which allows an upper frequency of approximately 2000 Hz, see Equation 2.1. Another requirement is that the microphone spacing shall be 81 mm $\pm$ 4 mm, which defines an approximate frequency range from 210 to 1900 Hz, see Equation 2.3 and 2.2 respectively. The in-situ test fixture as specified in the standard should practically be constructed with a wide outer dimension to be able to attach a sealing bed and to stand up-right onto the surface, see Figure 5.2 on the previous page. The fixture is attached, so that the inner diameter of the impedance tube is air tightly sealed-off to the atmosphere by filling the asphalt texture irregularities with a sealant material or an O-ring.

The contributions of measurement uncertainties are listed in ISO 13472-2:2011 Annex B. The mentioned sources of uncertainty are

- The normal incidence measurement method itself. This includes flaws of linearity in the microphone switching technique, the construction of the tube and all the signal processing devices.
- Deviations caused by measuring outside a well-controllable laboratory, such as meteorological variations and various external noise sources.
- The uncertainty of the reference measurement procedure. The parasitic absorption coefficient cannot be guaranteed to be stable throughout all the measured positions.
- The difference in air-leakage between the in-situ fixture and the asphalt for the averaged measurement positions.

The standard lists these uncertainties and suggests an estimated input quantity for each source of uncertainty. The suggested total standard uncertainty could then be added up to 0.015 and the expanded uncertainty to 0.029 at 95 % confidence level for all third-octave band frequencies of interest, see ISO 13472-2:2011 Annex B. Moreover, the standard mentions a general expression of a corrected sound absorption coefficient, where one add on all these mentioned uncertainties to the reference base corrected mean absorption coefficient. This general expression can be seen as a worst-case-scenario of the measurement reproducibility, and would in such case be useful as a proof of the demanded maximum surface layer absorption of 0.08 and 0.10 is fulfilled for the drive lane and propagation area respectively. Still, it should be mentioned that the expanded uncertainty is not a requirement by the standard, rather for informational use. In this thesis, the suggested expanded uncertainty is presented in all third-octave band filtered plots along with the standard deviation within the population.

## 5.4. Residual void content

For a regular road with dense asphalt concrete, DAC, the tyre/road noise can be reduced by constructing the surface to avoid high level peaks in the macro texture of the road surface. On the other hand, if the DAC is too even and smooth, the air drainage in the asphalt is reduced. This comes with the consequence of the amplifying horn effect between road surface and tyre, and ultimately a higher noise radiation from the tyre. Therefore, one must take in consideration to construct the road surface texture that combines both of these mentioned aspects for tyre/road noise reduction. In the case of heavy vehicle tyres, a rougher road surface texture can reduce the noise levels and differences between tyres. Also to mention is that the noise caused by the slip-stick motion and adhesive stick-snap is increased on an even and smooth surface, this is also true for the tonal components related to the pitch of the periodical thread pattern. [3] [22]

For an open porous asphalt, OPA, the acoustic sound absorption caused by inter-connected air voids in the surface layer is the most important surface characteristic that influences the vehicle noise in tests according to ISO 362-1. This is, as previously mentioned, due to the inter-connected air voids reduces the horn effect and ultimately the tyre/road noise. Moreover, the air drainage will work as a regular acoustic absorbent, the amount of reflected sound energy will be reduced from all sources of the vehicle. Due to this relation between air voids and sound absorption, one would either be able to measure the sound absorption coefficient or the residual void content, which is allowed according to ISO 10844:1994.

Residual void content can be described, similar to porosity, as the ratio of air volume to the total volume of the material. This can be seen as the percentage of air pockets situated in the surface layer, calculated as

$$\text{Void} = (1 - \frac{\rho_A}{\rho_R}) \cdot 100 \tag{5.1}$$

where $\rho_A$ and $\rho_R$ is the bulk density and theoretical density respectively,

$$\rho_A = \frac{m}{V} \tag{5.2}$$

where $m$ is the total mass of the drilled out core sample and $V$ is the volume excluding the volume of the air.

$$\rho_R = \frac{m_B + m_A}{V_B + V_A} \tag{5.3}$$

where the subscripts used are representing the two components of the asphalt, $A$ for aggregate and $B$ for binder.

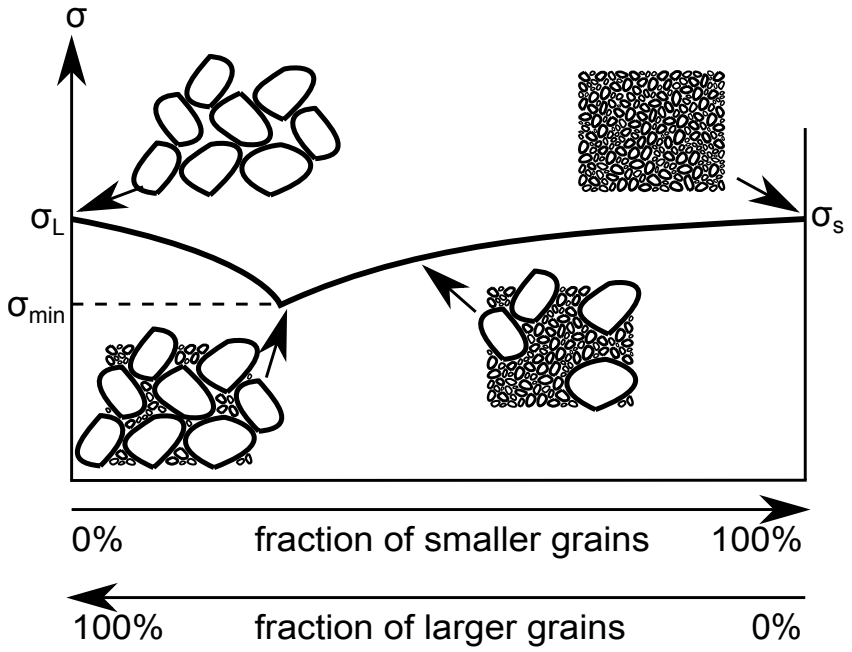


Figure 5.3.: Sketch of how the sieving of the stone chippings will create voids in the surface layer. This figure is adapted from reference [33].

The construction of open porous roads are not common, due to that the absorption effect is reduced after only a few years because debris are clogging the inter-connecting pores and that the softer binding material is worn out due to heavy vehicle traffic [22]. Moreover are the requirements of skid resistance often considered substandard on icy porous surfaces. So, instead of focusing on a high residual void content and the porosity, one could change the surface texture, altered by the sieving process, and the surface layer temperature at the road construction. The surface texture can be divided into macro and micro texture level, 0.5 mm to 50 mm and below 0.5 mm respectively. The stone chippings in the micro texture range are in direct contact with the tyre and can have a noise reducing effect if the texture is negative from the mean texture depth. The noise contribution due to the macro texture are on the other hand somewhat related to the type of vehicle. A texture that is optimized for a car could have an negative noise effect for heavy vehicle traffic. To produce a porous asphalt, the sieving should be done so that a range of stone chipping size is skipped, to make voids in the surface at a macro texture level, see Figure 5.3 . Another aging effect associated with porous asphalt layers is heat caused by direct sunlight [26]. At a specific temperature, the binding material is melting and will clog the negative macro texture in the surface that will decrease the inter-connecting voids at the deeper parts of the surface with the result of an increase noise level.

Figure 5.4.: Photo of performing the sand patch method. When this photo was taken, it just recently started to rain, hence the spots on the bright sand bed.

## 5.5. Mean texture depth, $MTD$

The mean texture depth, $MTD$, is describing the average depth in the macro texture range of a surface layer. This is measured by using the volumetric patch technique, also called the sand-patch method [3]. The concept is to pour out a given volume of a well defined type of fine sand mixture, i.e. solid glass spheres, on the surface layer, see Figure 5.4. A rubber pad, e.g. an ice-hockey puck, is used to circularly rub over the area with slight pressure, in order to spread out the sand patch to a circle until the rubber pad is nudging the surface of the highest level of aggregate. Since the volume of sand is known, one can divide this with the sand patch area to deduce the average macro texture depth,

$$MTD = \frac{4V}{\pi D^2} \tag{5.4}$$

where $V$ is the volume of sand mixture in milliliter and $D$ is the measured diameter in millimeter of the sand patch, averaged from four measurements per circle.

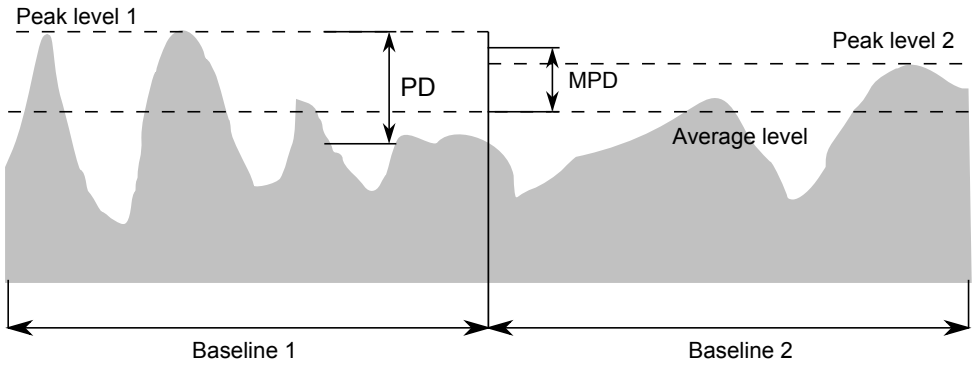


Figure 5.5.: Sketch of how the MPD measurement result should be interpreted and calculated.

## 5.6. Mean profile depth, $MPD$

The mean profile depth, $MPD$, described in the ISO 13473-1 [7] is an alternative method to the volumetric patch technique, see Section 5.5, to determine the average macro texture depth of a surface layer. The concept is to use a profilometer to measure a profile of the pavement texture in the macro texture range over a specified baseline of a given length, i.e. 100 mm. The standard specifies that the profilometer system should use a sensor technique that output an electrical signal proportional to the sensor reference plane, e.g. acoustical, laser, stylus, electro-optical type of sensor, see further in ISO 13473-2 [8]. This method is not as easily biased by the test technician, in comparison with the previously mentioned volumetric patch technique. The mean profile depth is obtained by arithmetically average the peak levels of the profile depth, $PD$, and subtract the average level, see the sketch in Figure 5.5. By using the estimated texture depth, $ETD$, one can approximate the $MTD$ with the $MPD$ by

$$MTD \approx ETD = 0.2\,mm + 0.8 \cdot MPD \tag{5.5}$$

## 5.7. Expected pass-by Noise level Difference from Texture level variation of road surface

The Expected pass-by Noise level Difference from Texture level variation of road surface, $END_T$, is a single number rating based on measurements of the texture profile relative to a reference surface. It can be seen as an estimation of the expected overall noise level radiated from the vehicle on the evaluated test track, based on the input of the texture profile and stated reference values. This measured texture profile is calculated to a third-octave texture profile spectrum, $L_{tx,\lambda}$, which includes the contribution

of the main two tyre/road noise generation mechanism [4]. The first is the texture induced structure-borne vibration of the tyre belt, caused by the impact of the tyre threads onto the road surface. The second is the air-pumping phenomenon, whereas the air is moving in and out of cavities of the tyre surface or between tyre threads and small void cavities in the road surface. [22]

The $END_T$ is calculated as,

$$END_T = 10log(\frac{A}{B}) - C \tag{5.6}$$

$$A = \sum 10^{(L_{mi}+b_i \cdot \Delta L_{tx,i})/10} \tag{5.7}$$

$$B = \sum 10^{L_{mi}/10} \tag{5.8}$$

$$C = 0.25\Delta L_{tx,5mm} \tag{5.9}$$

where $L_{mi}$ are the reference levels given in Table A.3, $b_i$ are the fixed factors given in Table A.4, $i = 1...13$ is the index corresponding to the third-octave center frequency 250 Hz to 4000 Hz, $\Delta L_{tx,i}$ are linearly interpolated as,

$$\Delta L_{tx,\lambda} = L_{tx,\lambda} - L_{tx,ref,\lambda} \tag{5.10}$$

where $\Delta L_{tx,\lambda}$ is the measured third-octave texture profile spectrum and $L_{tx,ref,\lambda}$ is the reference ISO 10844 Test Track spectrum given in Table A.2 in ISO 10844:2011. The subscript $5\,mm$ in $L_{tx,5mm}$ refer to the texture wavelength $\lambda = 5\,mm$.

The $END_T$ rating is not yet a normative part of ISO 10844:2011 since more results for validation is needed. Equation 5.6 is restricted to cases where elastic binding material is not used in the surface layer. If the surface layer would be considered as permeable, one should remove the term $C$ in the mentioned equation, since this represents the high frequency noise caused by the air-pumping phenomenon. [25]

# 6. Validation of the method by in-situ measurements

## 6.1. Reference measurement to validate the impedance tube

The in-situ measurement specified in ISO 13472-2:2011 requires a reference measurement to validate the equipment in use. This type of measurement is conducted with an empty impedance tube, i.e. the sample-end of the tube is rigidly terminated with a steel plate, see Figure A.1. The maximum absorption coefficient should not exceed 0.03 in any of the third-octave band central frequencies from 400 to 1600 Hz, that could occur due to the parasitic absorption caused by irregularities of the impedance tube inner wall and minor air leakages. The similar sealant material should be used for both the reference measurement and the measurement on the asphalt surface layer. In Figure A.2 to A.5 one can see the measured absorption coefficient, performed using both microphone spacing setups. From these plots one can deduce that that the 80 mm microphone spacing is the only one fulfilling the mentioned requirement. The reason for this difference is not due to the microphone spacing, rather the position of the microphones along the length of the tube. It is important that any microphone is not positioned in a pressure anti-mode, since this would result in a poor signal-to-noise ratio. To completely avoid these pressure anti-modes by carefully chosen microphone positions is not possible since there are numerous anti-modes in the frequency range of interest. One should rather focus on avoiding to position the microphones at lower frequency anti-modes, since the higher modes are multiples of the lower ones. In the plot of the average auto spectrum for the reference measurement using the 50 mm microphone spacing, see Figure A.6, one can see major magnitude dips in the frequencies 555 Hz, 952 Hz and 1296 Hz. These can also be seen in the corresponding coherence plot, see Figure A.7, i.e. the dips are a result of a measurement non-linearity between the microphone signals. For similar measurement using the 80 mm microphone spacing see Figure A.8 andA.9 respectively. Here, one can see major magnitude dips in the frequencies 437 Hz, 738 Hz and 1309 Hz.

It would be easy to calculate and relate the position of these pressure anti-modes by the well-known equations for resonances in pipes and ducts, however one must decide if the speaker-end of the tube should be defined as open or closed. One can assume that higher frequencies are reflected in the speaker membrane, though one also could argue

that the input noise signal to the speaker cone can result in an inter-modulated reflection. At lower frequencies one should include the effects of the absorption material-filled speaker-box behind the speaker cone, making the termination act as closed. In Figure A.10 and A.11 one can see plots of the first pressure anti-modes of interest in the tube, assuming that the speaker-end termination is closed respectively open. In these, one can see that microphone position A used in the 50 mm spacing is positioned in a point of many anti-modes. One can moreover see that the microphone position A, used in the 80 mm spacing, is also positioned in an anti-mode, although in a point of a high mode so it should not be seen as a problem. By this, one can assume that the 80 mm spacing is valid for in-situ measurements with this frequency range of interest.

Measurements were conducted without any sealant between the in-situ fixture and the surface layer, see Figure A.19. By this, one would be able to investigate the tendency of this air leakage and the maximum absorption coefficient this might be causing. As one can see, the increase in absorption coefficient is exclusively in the lower third-octave bands, whereas the upper third-octave bands could be comparable to a similar measurement conducted with sealant, see Figure A.21. As specified in ISO 10534-2, the standard for impedance tube measurements, the microphone closest to the sample should be positioned at least one lateral diameter from the sample surface; to guarantee that the only measured reflecting waves propagating from the sample are plane waves. In this case, where the in-situ fixture is unsealed, the higher frequencies have a sufficiently short wave length so that the non-plane waves have faded out at this distance, whereas the lower non-plane frequencies have a too long wavelength and will be added to the measurement result.

## 6.2. In-situ measurement on ISO 10844:1994 specified test track

In-situ measurements were conducted at a test patch next to AB Volvo's test track in Hällered. Since the test patch was constructed according to the ISO 10844:1994 standard, it requires that the absorption coefficient shall not exceed 0.10 at any point of the test surface. This measurement was done to prove that the developed impedance tube was able to obtain similar or reasonable values compared to previous measurements on the test track. In Figure A.12 to A.14 one can see the mean absorption coefficients of four measurement positions with three types of in-situ fixture sealants: Plastilina (petroleum modeling clay), Vaseline (petroleum jelly) and Tack-It (synthetic polymer including clay) respectively, where the plotted mean absorption coefficients are relative to the empty tube reference measurement on a steel plate. These specific sealant materials were chosen to investigate the sealing performance and the amount of remaining residue on the test surface after measurement, see photo in Figure A.15.

The measurement results are similar, however the Tack-It sealant result displays a slightly lower absorption coefficient for all the third-octave bands of interest. Moreover, from the mentioned figures one can see that Plastilina and Tack-It sealants shows a better standard deviation within the measured patches. The reason for this could be the material properties of the sealants. The Plastilina and Tack-It materials are in a more solid state in normal outdoor temperature than the Vaseline which can almost be considered slippery on the test surface. This becomes a problem if Vaseline is displaced into the patch to be measured, which can occur when the in-situ fixture is accidentally moved around when attaching it to the impedance tube. This would unintentionally seal the inter-connecting pores in parts of the test surface sample and absorption properties of the sealant would distort the measurement. Vaseline also leaves unwanted residue circular patches, as can be seen in Figure A.15, that will spread out to a greater sound reflecting patch if smeared out when driven over by a vehicle. One can also see that the Plastilina sealant also will leave a little quantity of residue. When returning to the measurement site after a month, the residue is still clearly visible, even though it have been subject to rain and most likely driven over by trucks, see Figure A.16. The Tack-It sealant is not included in these figures, as it did not leave any visual residue on the test site at all. This sealant can therefore be recommended to be used to measure without distorting the test track.

Tack-It was the only sealant used to measure in-situ at the actual propagation area of an ISO 10844:1994 test track, see Figure A.17, since it would not clog and distort the surface layer. By comparing these measurement results with the ones previously presented for the test patch, one can notice an increased absorption coefficient for the propagation area on the test track. These differences must be considered normal, since the test track has been regularly cleaned to remain at an absorption coefficient of 0.1, whereas the test patch is left uncleaned for many years, with the natural result of clogging with dust and other debris.

The plots in Figure A.18 displays a comparison of an in-situ measurement and an alternative way to measure the absorption coefficient on drilled out core samples. The latter samples are mounted into an impedance tube and measured according to ISO 10534-2, conducted by SP [13]. As one can see in the mentioned figure, the core sample measurement displays a lower absorption coefficient in all the third-octave bands of interest, however the measurement results are not strictly comparable due to some systematic errors; the core sample measurement was performed when the road surface was recently cleaned, in contrary to the in-situ measurement where the surface was suffering from wear, and the pores could be partly filled, however not clogged, with debris causing an increased absorption. When mounting the drilled out core samples in the impedance tube, a core sealant is used to make a tight seal to the inside wall of the tube. In this case, the sealant could have been applied in such way that it was causing parasitic sound absorption. In the in-situ measurement, there is always a mi-

nor parasitic absorption due to the included absorption of inter-connecting pores in the material outside of the intended lateral diameter. Moreover, as one can see in the previously mentioned figure, the noticeably higher standard deviation within the population of samples for the in-situ measurement can be solved by an even more precise sealing and repetitions.

## 6.3. In-situ measurement to relate the absorption with the texture depth

In-situ measurements were also performed on a dense asphalt concrete, a regular road and a porous asphalt to investigate if the measured mean texture depth, $MTD$, can be directly related to the measured absorption coefficient. In Figure A.17 and A.20 to A.22 one can see the plots of the measured absorption coefficient filtered in third-octave bands for the separate measurement sites. Photos of the surface layers on the measurement sites can be seen in Figure A.23 to A.26, where all the measurements were conducted on the propagation part of the road surface. The sound absorption coefficient, averaged as according to ISO 10844:1994 and ISO 10844:2011 see Section 5.2, is presented together with the measured mean texture depth, $MTD$, and the approximated mean profile depth, $MPD$, in Table A.1 on page 55.

In this table, it is easy to interpret the relation between the $MTD$ and the photos of the measurement sites; the mean texture depth is increasing with the roughness of the surface as can be seen in the mentioned photos. However, this relation cannot be seen when relating the $MTD$ to the measured sound absorption coefficients, despite the different type of average calculations. Instead, by relating the $MTD$ with the plots of the third-octave band filtered sound absorption for the different measurement sites, see the figure references in the mentioned table, one can see that the regular road concrete and the dense asphalt concrete displays similar measurement results, despite that the $MTD$ for the regular road concrete is twice as deep. Moreover, one can deduce that the porous asphalt have a $MTD$ that is much deeper than the other surfaces, but still show a sound absorption similar to the other surfaces in the high frequency region, from 800 Hz to 1600 Hz, and a lower absorption in the lower frequency region from 400 Hz to 800 Hz. The latter region displays a poor standard deviation compared to the other measurements, since the sealant was not correctly applied for all the measurements at this site. That the sound absorption is increased in the lower frequency range, if the sealant is not correctly applied, can also be seen Figure A.19, where no sealant was used between the in-situ fixture and the surface. The measured porous asphalt is situated at road Högsboleden in Gothenburg and was constructed year 2006. The absorption efficiency after six years are expected to decrease, although this measurement was conducted in the propagation area and not in a drive lane.

In the mentioned TableA.1, one can see that the in-situ and core sample measurements of the test track have equal mean sound absorption coefficient averages according to ISO 10844:2011. As previously mentioned in Section 5.2, the propagation area must be measured to a maximum absorption coefficient of 0.10, which should be fulfilled by each third-octave band in the range from 315 Hz to 1600 Hz. Note that the mentioned standard do not specify that the highest absorption coefficient shall be presented as a single value, this is done in this thesis for comparison purposes only. All third-octave bands of interest should rather be presented as a graph or table, which seems natural if one would compare the plots in Figure A.18, used as input data in TableA.1.

The mean profile depth, $MPD$, should be measured to be 0.5 mm $\pm$ 0.2 mm in the driving lane, according to ISO 10844:2011. All the approximated values for the different measurement sites in Table A.1 are above these values, although the $MPD$ for the dense asphalt concrete is inside the vicinity of the required value. The $MTD$ was excluded in the revised ISO 10844:2011 standard, since it was thought that the measurement procedure could be intentionally, or unintentionally, biased by the test technician. The test could be underestimated if the test technician applies to little force that the rubber pad is almost not touching the highest peak of aggregate. The test could also be underestimated if the test technician is not careful that all of the sand mixture is leveled out.

# 7. Validation of the three-microphone method

## 7.1. Two-microphone vs. three-microphone measurement method

A comparison was performed to relate the well-known ISO 10534-2:1998 standard using two microphones with a method using three microphones, as described in Chapter 2 and 3 respectively. The two methods were conducted to correspond as much as possible with the only discrepancy of the rigid end-piece backing the sample, i.e. the measurements were performed on a single sample that was not refitted between each measurement. In Figure B.1 and B.4 one can see the measurement results of these measurements, and it is clear that the absorption and coherence are similar for the two measurement methods. The absorption material sample was initially covered by a thin plastic screen and attached onto a heavy layer with an adhesive. These were carefully removed to ensure that the material could be assumed isotropic. As one can see in the mentioned figure, a clear resonance is appearing at approximately 500 Hz, one can by this assume that the top layer of the absorption panel is still covered by glue which could act as a mass in a mass-spring system. This phenomena is discussed in [35], where it is suggested to suppress these resonant vibrations by fixating multiple thin nails from the surface to the rigid end of the sample. The external company Matelys have presented measurement results [27] for samples extracted from the same unique material as previously discussed. Looking at the grey dispersion plot in the left subfigure in Figure 2 on page 10 in [27], one can draw the conclusion that the measurement results are similar to the absorption coefficient results plotted in Figure B.1 and B.3.

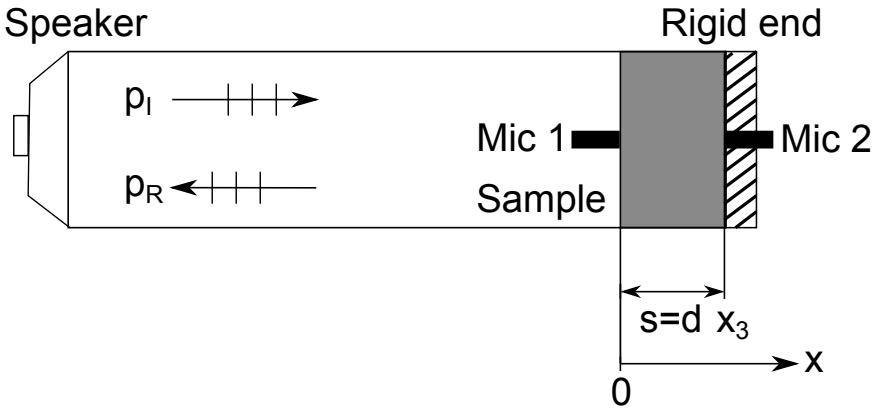


Figure 7.1.: A sketch of the impedance tube configuration using two microphones close to the surface at each side of the sample.

## 7.2. Additional acoustic parameters using the three-microphone measurement method

Using the three-microphone method presented in Chapter 3, one should be able to obtain various acoustic material parameters. The investigated sample is similar to the one used in the previous section. In addition to this, the sample is assumed to be an homogenous and isotropic porous non-woven material for which the acoustic and non-acoustic parameters are well documented, see data in Table B.1.

The calculated complex wave number and normalized characteristic impedance using the three-microphone method can be seen in Figure B.5 and B.6. In both figures one can also so see a plot based on the empirical model of Delany & Bazley, with a modeled flow resistivity of 20000 $\mathrm{N{\cdot}s{\cdot}m^{-4}}$, and the measurement result of an so-called inside tube measurement. The latter was conducted by the setup of a microphone at the sample surface, $x = 0$, and one at the rigid backing, $x = d$, to directly measure the $H_{30}$ transfer function over the actual material, including the usage of the microphone switching technique as described in Chapter 2. See a sketch of the mentioned setup in Figure 7.1. By using this method, one is able to measure the accurate $H_{30}$ transfer function, which in the three-microphone method case have to be calculated by Equation 3.2 to 3.8. These $H_{30}$ transfer functions are compared in Figure B.7, from which one can deduce that the transfer functions are not similar and one can conclude that the calculations in the three-microphone method is not equal to the measured $H_{30}$. Moreover, by comparing the plots in Figure B.5 and B.6 one can see that the direct measurement of the $H_{30}$ transfer function has a curvature in the similar range as the plot based on the empirical model of Delany & Bazley.

More acoustic and non-acoustic parameters, described in Chapter 3 and 4, have been calculated using the $H_{30}$ transfer function obtained using the inside tube measurement, see Table B.1. In the first row of this table, the single values are the means of the entire valid frequency range. In comparison to the calculations and measurements made on the similar material by the external company Matelys, see the second row of the mentioned table, one can conclude that some of the obtained values are reasonable and in the similar range. Deviations between the measurements are expected, since the measured sample could still include some adhesive that would close pores and add mass at both surfaces and the sample is not equally compressed throughout the material. Hence, the initial assumption that the material is homogenous and isotropic is not valid.

In summary, the alternative three-microphone method did not show measurement results that was useful to obtain additional acoustic and non-acoustic material results. However, it was shown that by measuring the $H_{03}$ transfer function, one could show calculations results that are reasonable and in the similar range as those made by an external company.

# 8. Conclusion

The developed impedance tube measurement method can be considered as valid for absorption material measurement and in-situ measurement on road surfaces, according to the current standards ISO 10534-2:1996 and ISO 13472-2:2011 respectively. In comparison to external measurement results using other equipment, the developed impedance tube shows similar and reasonable absorption coefficient results for the in-situ method. It was shown that the position of the microphones in the tube is important to obtain an acceptable signal to noise ratio for further calculations using the transfer function method.

In-situ measurement results on road surfaces showed the importance of the sealing method and the choice of sealant. It was shown that Plastilina (petroleum modeling clay) and Tack-It (synthetic polymer including clay) sealants are two preferred sealants. In addition to a low standard deviation within population, these two also holds the properties of being in a solid state in normal outdoor temperature and leaves low amount of residue after a completed measurement. The Tack-It sealant can be recommended if no sealant residue is allowed to be left on the test track.

In the revised ISO 10844:2011, the Mean Texture Depth, $MTP$, is replaced by Mean Profile Depth, $MPD$. Although the latter was only approximated, one could determine that the $MTP$ for the measured test track should be lowered to pass the new requirements. The investigation of the relation between Mean Profile Depth, $MTD$, and the normal incidence sound absorption coefficient showed that they are not related for regular road asphalt surfaces.

The alternative three-microphone method did not show measurement results that were useful to obtain additional acoustic and non-acoustic material results. However, it was shown that by measuring the $H_{03}$ transfer function, one could show results that are reasonable and in the similar range as external measurements.

# Bibliography


[1] ISO 10534-1:1996. Acoustics - determination of sound absorption coefficient and impedance in impedances tubes - part 1: Method using standing wave ratio, 1996.

[2] ISO 10534-2:1998. Acoustics - determination of sound absorption coefficient and impedance in impedances tubes - part 2: Transfer-function method, 1998.

[3] ISO 10844:1994. Acoustics - specification of test tracks for the purpose of measuring noise emitted by road vehicles, 1994.

[4] ISO 10844:2011. Acoustics - specification of test tracks for measuring noise emitted by road vehicles and their tyres, 2011.

[5] EN 13036-7:2003. Road and airfield surface characteristics - test methods - part 7: Irregularity measurement of pavement courses: the straightedge test, 2003.

[6] ISO 13472-2:2011. Acoustics - measurement of sound absorption properties of road surfaces in situ - part 2: Spot method for reflective surfaces, 2011.

[7] ISO 13473-1:1997. Characterization of pavement texture by use of surface profiles - part 1: Determination of mean profile depth, 1997.

[8] ISO 13473-2:2011. Characterization of pavement texture by use of surface profiles - part 2: Terminology and basic requirements related to pavement texture profile analysis, 2002.

[9] ISO 29053:1993. Acoustics - materials for acoustical applications - determination of airflow resistance, 1993.

[10] ISO 362-1:2007. Measurement of noise emitted y accelerating road vehicles - engineering method - part 1: M and n catergories, 2007.

[11] ECE Regulation No. 51.02. Noise of m and n categories of vehicles, 1995.

[12] J.F. Allard and N. Atalla. *Propagation of sound in porous media : modelling sound absorbing materials*. John Wiley & Sons, Ltd, second editon edition, 2009.

[13] H Andersson. Determination of sound absorption coefficient. Technical Report P402052-1 Appendix 1, SP, 2004.

[14] Noureddine Atalla, Raymond Panneton, and Patricia Debergue. A mixed displacement-pressure formulation for poroelastic materials. *The Journal of the Acoustical Society of America*, 104(3):1444–1452, 1998.

[15] M. A. Biot. Theory of propagation of elastic waves in a fluid-saturated porous solid. i. low-frequency range. *The Journal of the Acoustical Society of America*, 28(2):168–178, 1956.

[16] M. A. Biot. Theory of propagation of elastic waves in a fluid-saturated porous solid. ii. higher frequency range. *The Journal of the Acoustical Society of America*, 28(2):179–191, 1956.

[17] Carl-Axel Carlsson. The current iso asphalt at hllered has deteriorated by 1.75 db since 1997. new asphalt was therefore applied in july 2004. sound absorption tests show that the iso asphalt successfully has been restored to about the same level as in 1997. Technical Report ER-600967, Volvo AB, 2004.

[18] Carl-Axel Carlsson. Comparison of iso noise test tracks at michelin, la valbonne and hllered. fh-615 was used as test object as well as a reference sound source. michelin new p-49 noise track is the best choise provided it will be approved by the authorities. Technical Report ER-626876, Volvo AB, 2012.

[19] J. Y. Chung and D. A. Blaser. Transfer function method of measuring in-duct acoustic properties. i. theory. *The Journal of the Acoustical Society of America*, 68(3):907–913, 1980.

[20] Trevor J Cox and Peter D'Antonio. *Acoustic absorbers and diffusers: theory, design, and application*. Taylor & Francis, second edition edition, 2009.

[21] Olivier Doutres, Yacoubou Salissou, Noureddine Atalla, and Raymond Panneton. Evaluation of the acoustic and non-acoustic properties of sound absorbing materials using a three-microphone impedance tube. *Applied Acoustics*, 71(6):506 – 509, 2010.

[22] Ulf Sandberg Jerzy A. Ejsmont. *Tyre/Road noise reference book*. INFORMEX, first edition, 2002.

[23] David Linton Johnson, Joel Koplik, and Roger Dashen. Theory of dynamic permeability and tortuosity in fluid-saturated porous media. *Journal of Fluid Mechanics*, 176:379–402, 1987.

[24] Michael R. F. Kidner and Colin H. Hansen. A comparison and review of theories of the acoustics of porous materials. *International Journal of Acoustics and Vibration*, 13:112–119, 2008.

[25] P. Klein and J-F Hamet. Endt : Expected pass-by noise level difference from texture level variation of the road surface. Technical report, SILVIA, 2005.

[26] S Konishi and T Ozaki. Age influence of tire/road noise on iso test track. In *Inter noise 98*, 1998.

[27] Francois-Xavier Becot Luc Jaouen. Optimisation of the acoustica absorption of non-woven noise shields, phase 3: Uni-axial compression f porous media: modeling and applications to fibrous materials. Technical report, MATELYS, 2009.

[28] Xavier Olny and Raymond Panneton. Acoustical determination of the parameters governing thermal dissipation in porous media. *The Journal of the Acoustical Society of America*, 123(2):814–824, 2008.

[29] Raymond Panneton. Comments on the limp frame equivalent fluid model for porous media. *The Journal of the Acoustical Society of America*, 122(6):EL217–EL222, 2007.

[30] Raymond Panneton and Xavier Olny. Acoustical determination of the parameters governing viscous dissipation in porous media. *The Journal of the Acoustical Society of America*, 119(4):2027–2040, 2006.

[31] X. Sagartzazu, L. Hervella-Nieto, and J. Pagalday. Review in sound absorbing materials. *Archives of Computational Methods in Engineering*, 15:311–342, 2007. 10.1007/s11831-008-9022-1.

[32] Yacoubou Salissou and Raymond Panneton. Wideband characterization of the complex wave number and characteristic impedance of sound absorbers. *The Journal of the Acoustical Society of America*, 128(5):2868–2876, 2010.

[33] Ennes Sarradj, Tobias Lerch, and Jrn Hbelt. Input parameters for the prediction of acoustical properties of open porous asphalt. *Acta Acustica united with Acustica*, 92:8596, 2006.

[34] Bryan H. Song and J. Stuart Bolton. A transfer-matrix approach for estimating the characteristic impedance and wave numbers of limp and rigid porous materials. *The Journal of the Acoustical Society of America*, 107(3):1131–1152, 2000.

[35] Y. Izumi T. Iwase and R. Kawabata. A new measuring method for sound propagation constant by using sound tube without any air spaces back of a test material. In *INTERNOISE 98*, 1998.

[36] Martin Wolkesson. Sound absorption measurements in impedance tube. Instruction L47-P9-05, Volvo Noise&Vibration Laboratory, AB Volvo, 2013.

# A. Two-microphone method measurement results

Figure A.1.: Photo of the in-situ test fixture attached to a thick steel plate used to perform an empty tube measurement.

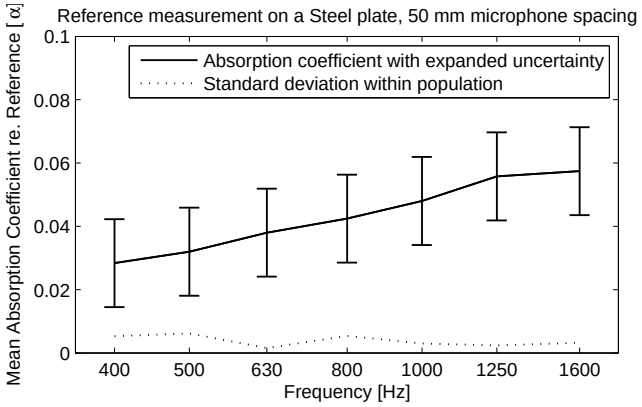


Figure A.2.: Plot of the mean absorption coefficient, filtered in third-octave bands, from an in-situ measurement on a steel plate. The microphones were setup in the 50 mm spacing.

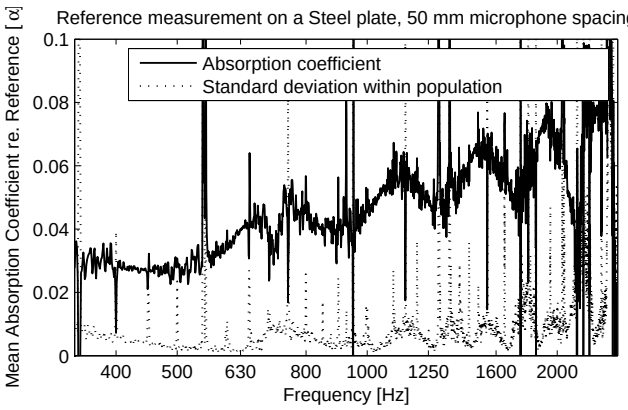


Figure A.3.: Plot of the mean absorption coefficient from an in-situ measurement on a steel plate. The microphones were setup in the 50 mm spacing.

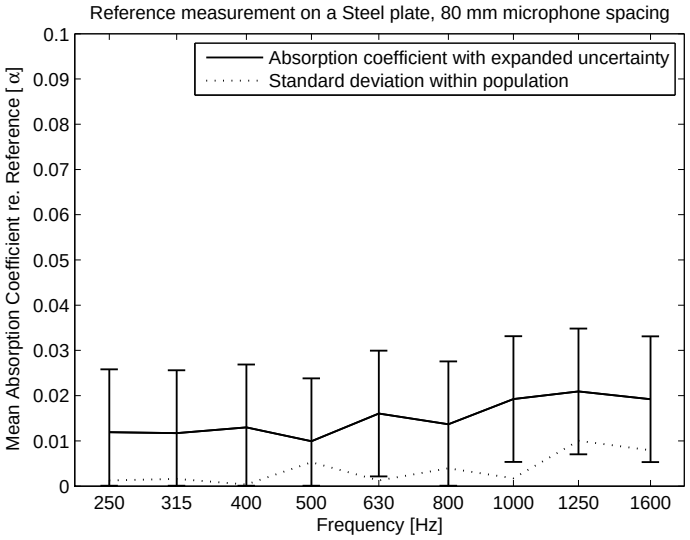


Figure A.4.: Plot of the mean absorption coefficient, filtered in third-octave bands, from an in-situ measurement on a steel plate. The microphones were setup in the 80 mm spacing.

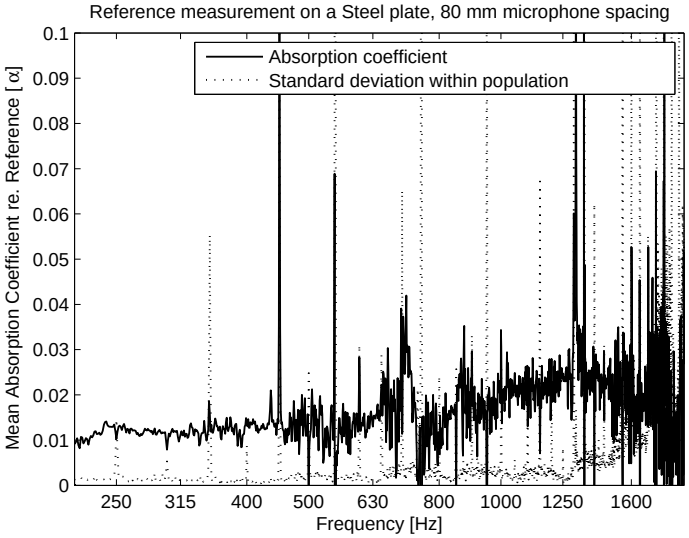


Figure A.5.: Plot of the mean absorption coefficient from an in-situ measurement on a steel plate. The microphones were setup in the 80 mm spacing.

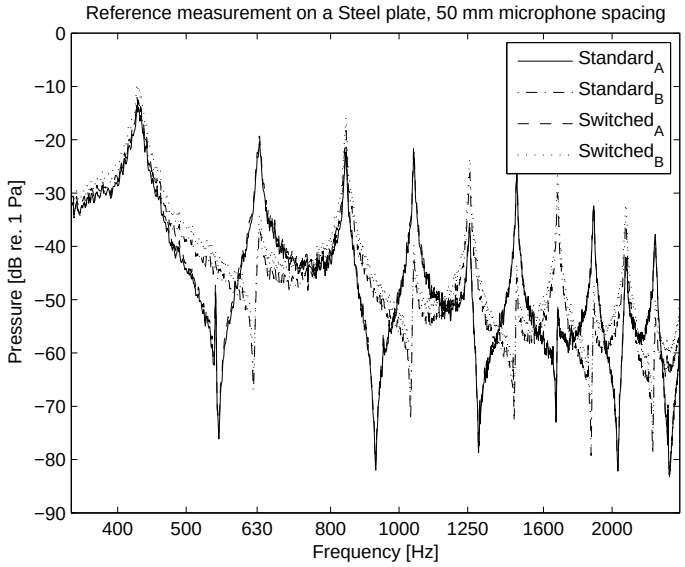


Figure A.6.: Plot of the averaged auto spectrum from an in-situ measurement on a steel plate. The microphones were setup in the 50 mm spacing.

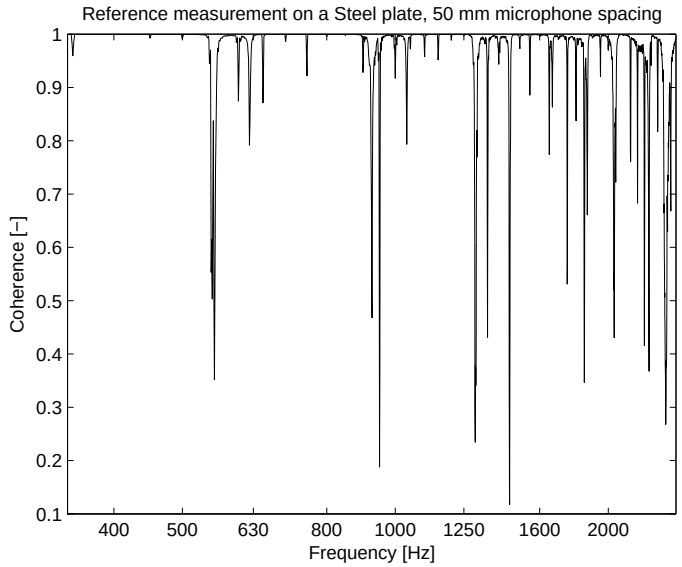


Figure A.7.: Plot of the averaged auto spectrum from an in-situ measurement on a steel plate. The microphones were setup in the 50 mm spacing.

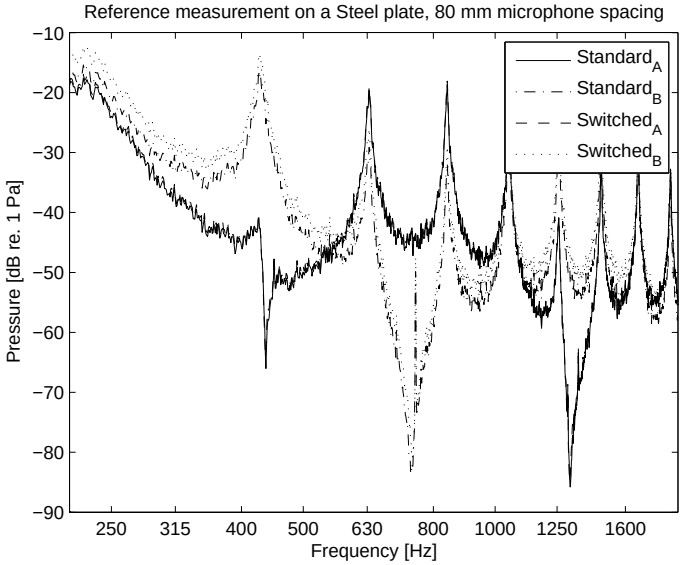


Figure A.8.: Plot of the averaged auto spectrum from an in-situ measurement on a steel plate. The microphones were setup in the 80 mm spacing.

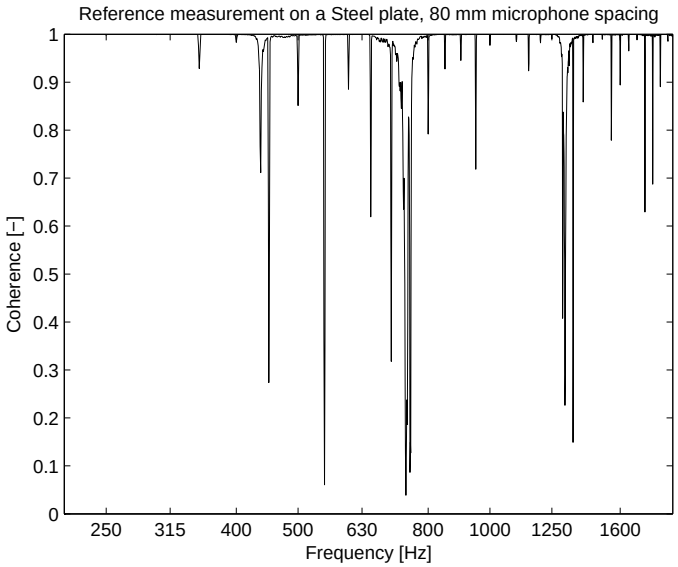


Figure A.9.: Plot of the averaged auto spectrum from an in-situ measurement on a steel plate. The microphones were setup in the 80 mm spacing.

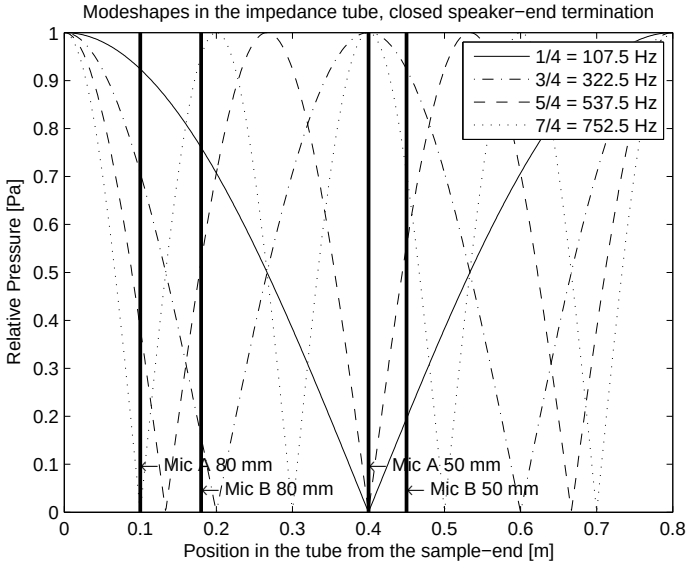


Figure A.10.: Mode-shapes in the impedance tube if the speaker-end termination is assumed closed

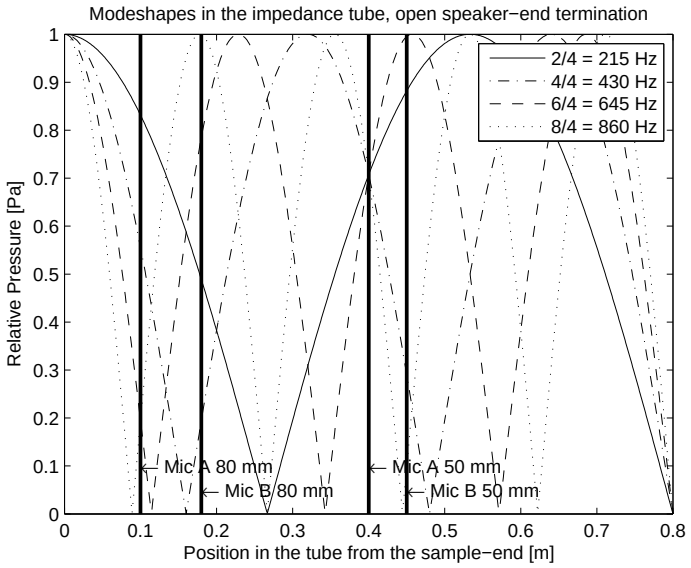


Figure A.11.: Modes-shapes in the impedance tube if the speaker-end termination is assumed open

Table A.1.: Table of mean of maximum absorption, $\alpha_{1994}$, absorption coefficient, $\alpha_{2011}$, mean texture depth, $MTD$, and the approximated mean profile depth, $MPD$. The latter is obtained according to Equation 5.5.

| Measurement site (Figure reference) | $\alpha_{1994}$ [-] | $\alpha_{2011}$[-] | $MTD$ [mm] | $MPD$ [mm] |
|---|---|---|---|---|
| ISO 10844:1994 test track, in-situ (A.18) | 0.10 | 0.10 | 1.1 [18] | 1.08 |
| ISO 10844:1994 test track, drilled core(A.18) | 0.08 | 0.10 | 0.91 [17] | 0.93 |
| Dense asphalt concrete (A.20) | 0.03 | 0.03 | 0.63 | 0.70 |
| Regular road concrete (A.20) | 0.03 | 0.04 | 1.22 | 1.18 |
| Porous asphalt (A.20) | 0.03 | 0.03 | 1.86 | 1.69 |

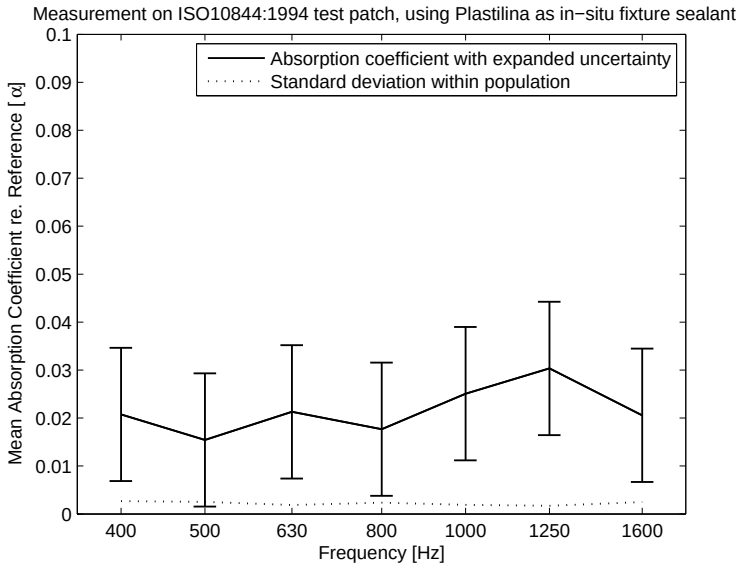


Figure A.12.: Plot of an in-situ measurement on a ISO 10844:1994 test track, filtered in third-octave bands. Plastilina was used as in-situ fixture sealant to the road surface.

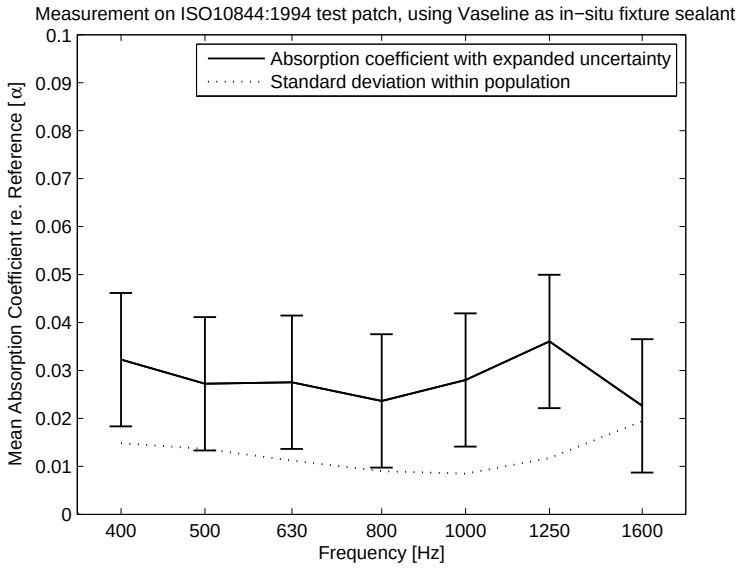


Figure A.13.: Plot of an in-situ measurement on a ISO 10844:1994 test track, filtered in third-octave bands. Vaseline was used as in-situ fixture sealant to the road surface.

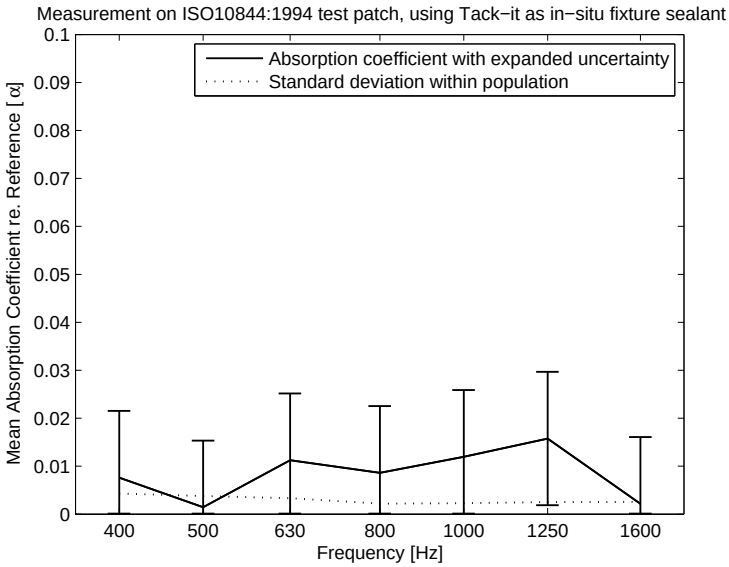


Figure A.14.: Plot of an in-situ measurement on a ISO 10844:1994 test track, filtered in third-octave bands. Vaseline was used as in-situ fixture sealant to the road surface.

Figure A.15.: Photo of the test surface used for the in-situ measurement on a test patch. The eight circles is the in-situ sealant residue patches. The upper three patches seen in the photo is the residue from Plastilina, whereas the lower four are from Vaseline. In the upper left corner one can see the lower part of the impedance tube while performing a measurement.

Figure A.16.: Photo of the test patch one month after the measurement case shown in Figure A.15.

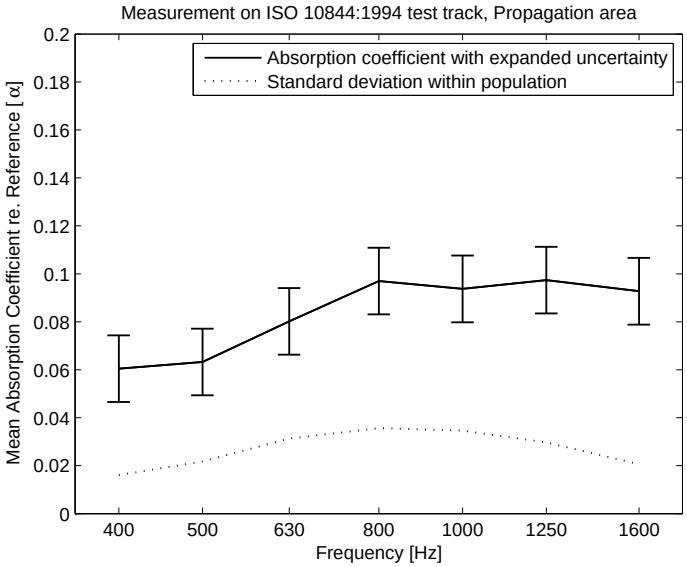


Figure A.17.: Plot of an in-situ measurement on the propagation area of an a ISO 10844:1994 test track, filtered in third-octave bands. Tack-it was used as in-situ fixture sealant to the road surface. Note the y-axis limitation from 0 to 0.2.

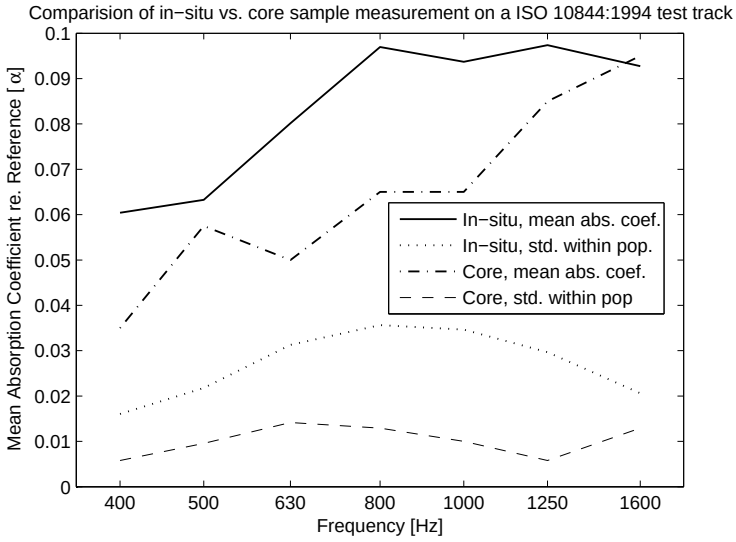


Figure A.18.: Comparison plot of an in-situ measurement, using Plastilina as sealant, versus a drilled out core sample fitted into an impedance tube. The mean is made over a population of four samples for both the in-situ and core measurements.

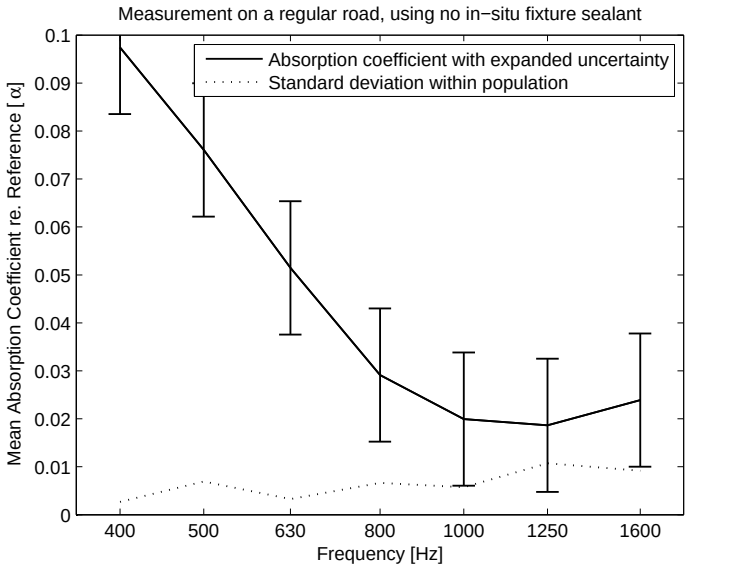


Figure A.19.: Plot of an in-situ measurement on a regular, filtered in third-octave bands. No sealant was applied between the in-situ fixture and the surface layer.

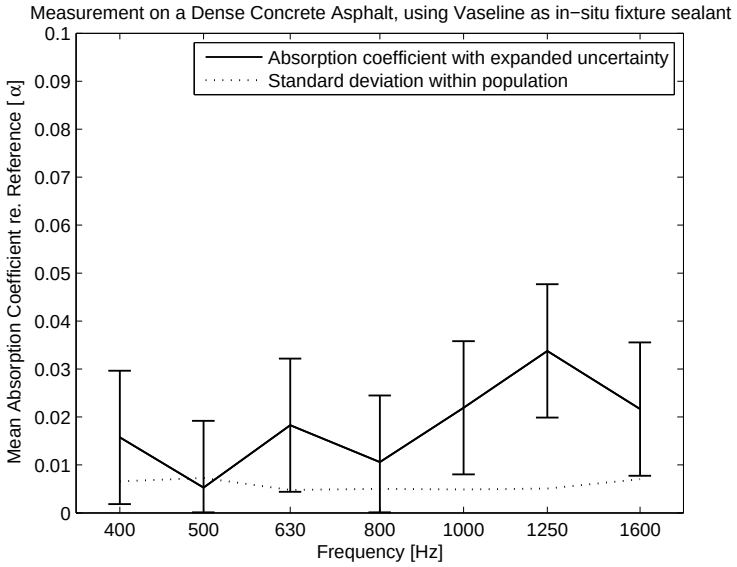


Figure A.20.: Plot of an in-situ measurement on a Dense Concrete Asphalt, filtered in third-octave bands. Vaseline was used as in-situ fixture sealant to the road surface.

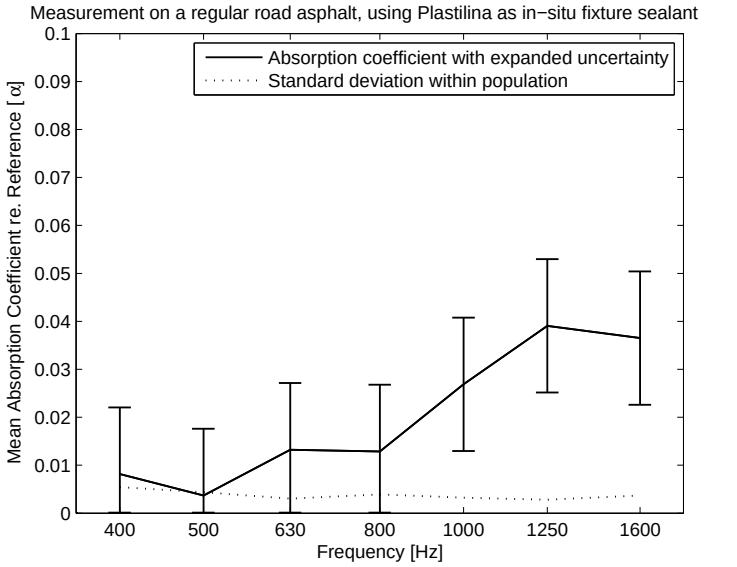


Figure A.21.: Plot of an in-situ measurement on a regular road, filtered in third-octave bands. Plastilina was used as in-situ fixture sealant to the road surface.

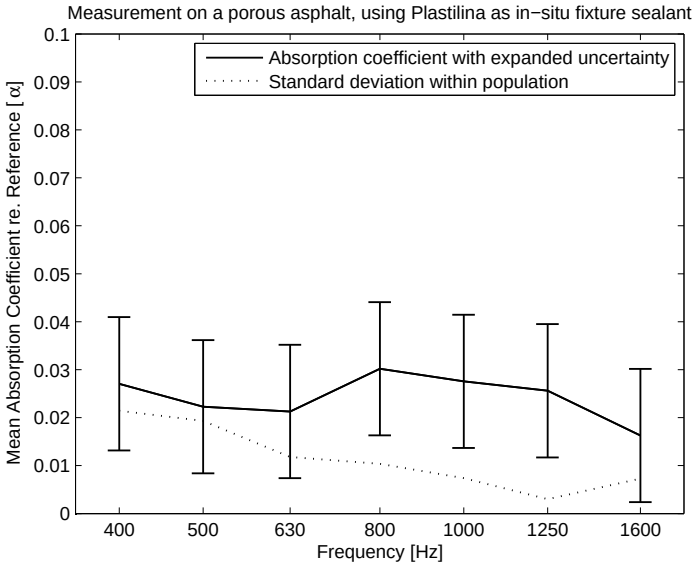


Figure A.22.: Plot of an in-situ measurement on a porous asphalt, filtered in third-octave bands. Plastilina was used as in-situ fixture sealant to the road surface.

Figure A.23.: Photo of the ISO 10844:1994 specified test track surface layer. The inner diameter of the sealant circle is 80 mm. This photo shows the Tack-It sealant between the in-situ fixture and the surface layer. This sealant will be removed completely resulting in no residual debris, as seen for other sealants in Figure A.15.

Figure A.24.: Photo of the measured dense asphalt concrete surface layer. The inner diameter of the sealant circle is 80 mm.

Figure A.25.: Photo of the measured regular road surface layer. The inner diameter of the sealant circle is 80 mm.

Figure A.26.: Photo of the measured porous asphalt surface layer. The inner diameter of the sealant circle is 80 mm.

# B. Three-microphone method measurement results

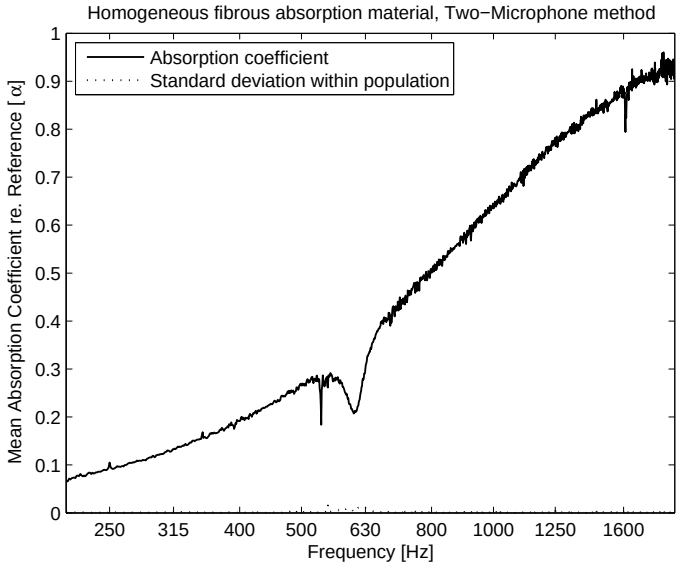


Figure B.1.: Plot of the mean absorption coefficient of a homogenous fibrous absorption material, using the two-microphone method. Note that the standard deviation within population is close to zero in the shown frequency range.

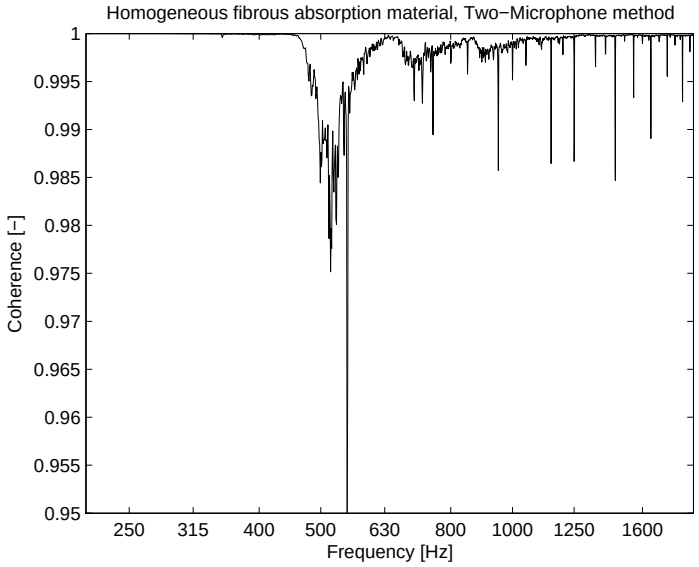


Figure B.2.: Plot of the coherence of a homogenous fibrous absorption material, using the two-microphone method.

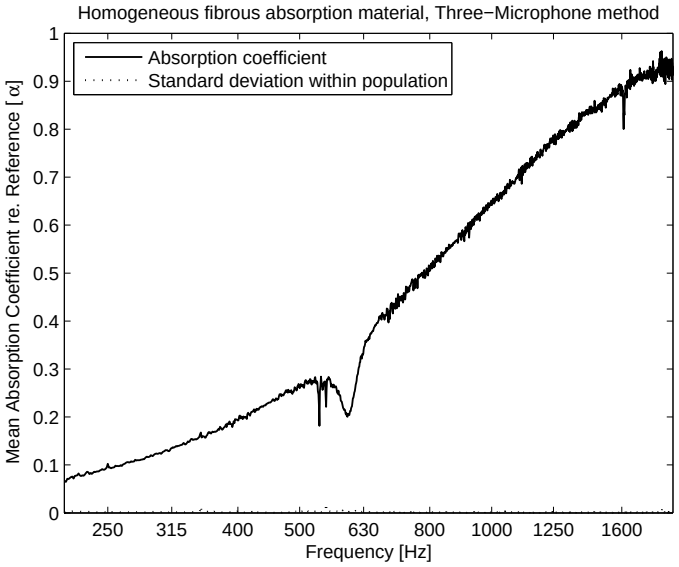


Figure B.3.: Plot of the mean absorption coefficient of a homogenous fibrous absorption material, using the three-microphone method. Note that the standard deviation within population is close to zero in the shown frequency range.

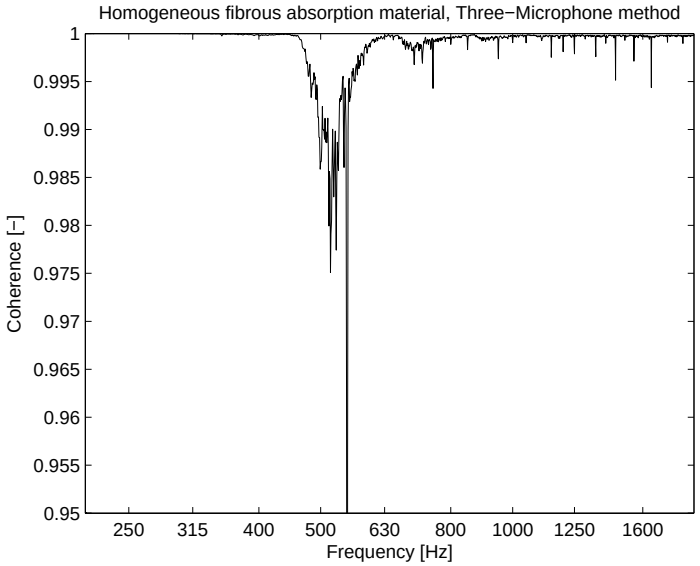


Figure B.4.: Plot of the coherence of a homogenous fibrous absorption material, using the three-microphone method.

| Result | d | $\sigma$ | $\phi$ | $\alpha_\infty$ | $\Lambda$ | $\Lambda'$ | $E$ | $\eta$ | $\rho$ |
|---|---|---|---|---|---|---|---|---|---|
| Unit | mm | $\mathrm{N{\cdot}s{\cdot}m^{-4}}$ | - | - | $\mu$m | $\mu$m | $\mathrm{10^3 N{\cdot}m^{-2}}$ | - | $\mathrm{kg{\cdot}m^{-3}}$ |
| Thesis | 30 | 3323 | - | 1.71 | 102 | 26437 | 97 | - | - |
| Matelys | 30 | 19700 | 0.96 | 1.01 | 104 | 116 | 55 | 0.08 | 81 |

Table B.1.: Table of characteristics of acoustic and non-acoustic parameters. The second row is made by an external company and adapted from Table 1 in reference [27], denoted as "Felt 30 mm - characterization".

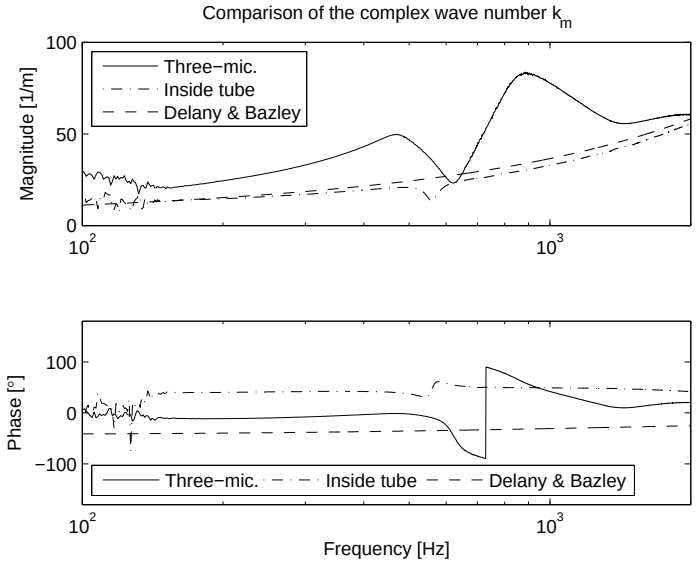


Figure B.5.: Comparison plot of the calculated complex wave number of the material and the empirical Delany and Bazley model.

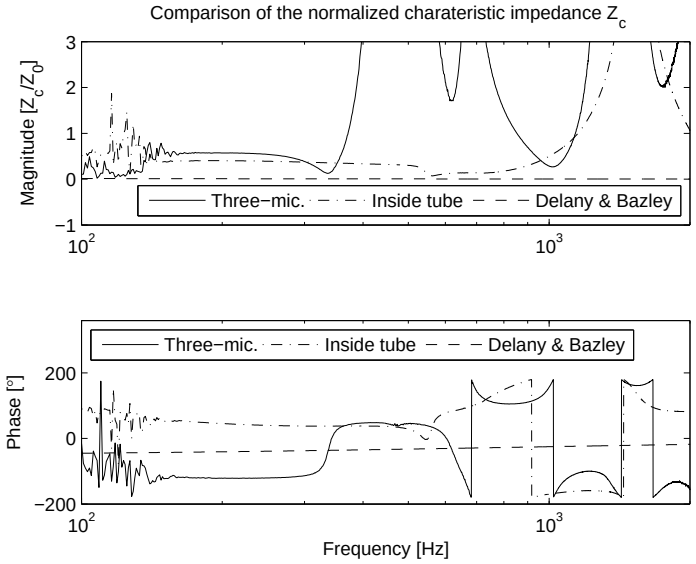


Figure B.6.: Comparison plot of the normalized characteristic impedance of the material and the empirical Delany and Bazley model.

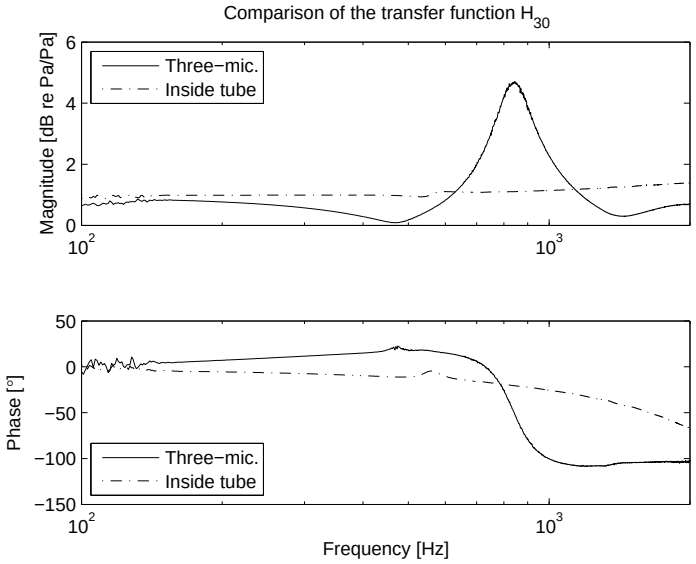


Figure B.7.: Comparison plot of the transfer function $H_{30}$ obtained by the three-microphone method compared to the direct measurement inside the tube.